RESEARCH ARTICLE

# Pharmacogenomic Profiling of Pediatric Acute Myeloid Leukemia to Identify Therapeutic Vulnerabilities and Inform Functional Precision Medicine

Han Wang[1], Kathy Yuen Yee Chan[1], Chi Keung Cheng[2], Margaret H.L. Ng[2], Po Yi Lee[1], Frankie Wai Tsoi Cheng[3], Grace Kee See Lam[3], Tin Wai Chow[3], Shau Yin Ha[4], Alan K.S. Chiang[4], Wing Hang Leung[4], Anskar Y.H. Leung[5], Chi Chiu Wang[6], Tao Zhang[6], Xiao-Bing Zhang[7], Chi Chiu So[8], Yuet Ping Yuen[8], Qiwei Sun[1], Chi Zhang[1], Yaqun Xu[1], John Tak Kit Cheung[1], Wing Hei Ng[1], Patrick Ming-Kuen Tang[2], Wei Kang[2], Ka-Fai To[2], Wayne Yuk Wai Lee[9], Raymond S.M. Wong[10], Ellen Ngar Yun Poon[11], Qi Zhao[12], Junbin Huang[13], Chun Chen[13], Patrick Man Pan Yuen[1], Chi-kong Li[1,14], Alex Wing Kwan Leung[1,14], and Kam Tong Leung[1,14]

**ABSTRACT** Despite the expanding portfolio of targeted therapies for adults with acute myeloid leukemia (AML), direct implementation in children is challenging due to inherent differences in underlying genetics. Here we established the pharmacologic profile of pediatric AML by screening myeloblast sensitivity to approved and investigational agents, revealing candidates of immediate clinical relevance. Drug responses *ex vivo* correlated with patient characteristics, exhibited age-specific alterations, and concorded with activities in xenograft models. Integration with genomic data uncovered new gene–drug associations, suggesting actionable therapeutic vulnerabilities. Transcriptome profiling further identified gene-expression signatures associated with on- and off-target drug responses. We also demonstrated the feasibility of drug screening–guided treatment for children with high-risk AML, with two evaluable cases achieving remission. Collectively, this study offers a high-dimensional gene–drug clinical data set that could be leveraged to research the unique biology of pediatric AML and sets the stage for realizing functional precision medicine for the clinical management of the disease.

**SIGNIFICANCE:** We conducted integrated drug and genomic profiling of patient biopsies to build the functional genomic landscape of pediatric AML. Age-specific differences in drug response and new gene–drug interactions were identified. The feasibility of functional precision medicine–guided management of children with high-risk AML was successfully demonstrated in two evaluable clinical cases.

## INTRODUCTION

Acute myeloid leukemia (AML) is a rare but aggressive hematologic malignancy that accounts for ~5% of pediatric cancers (1). For decades, intensive chemotherapy based on anthracyclines and cytarabine with or without hematopoietic stem cell transplantation (HSCT) has remained the standard of care (2). Advances in the risk-adapted application of these regimens have significantly improved the overall survival of newly diagnosed AML to ~70% (3, 4). However, a substantial proportion of patients relapse, with <40% of whom can be cured with reinduction or salvage therapies (5). Further intensification of existing chemotherapeutic regimens is unlikely to result in a major reduction in relapse or a significant improvement in overall survival without incurring excessive toxicity. The advent of effective therapies is, therefore, crucial but it is improbable to succeed by a simple extrapolation of new agents approved for adult AML because of the largely different genetics and biology (6, 7).

Precision medicine refers to the tailoring of specific medications to different individuals for a given disease instead of adopting the one-size-fits-all approach (8). In the cancer field, it is nearly synonymous with genomics. Efforts in large-scale genomic sequencing have revealed AML as a genetically heterogeneous disease that comprises multiple subclasses with distinct outcomes (9, 10). Targetable lesions, such as *FLT3* and *IDH1/2*, were identified and translated into revolutionary therapies. The Beat AML alliance prospectively enrolled patients with AML ≥60 years of age with genetic analyses completed within a week from diagnosis and demonstrated superior survival in those receiving genomic-based treatment relative to standard of care (11). The genomic landscape of pediatric AML has also been extensively characterized, which revealed disproportionately prevalent lesions in young individuals as opposed to adults (6, 12, 13). In connection, the LEAP consortium recently reported the integration of genomic discoveries into clinical care for children with

[1]Department of Paediatrics, The Chinese University of Hong Kong, Shatin, Hong Kong. [2]Department of Anatomical and Cellular Pathology, The Chinese University of Hong Kong, Shatin, Hong Kong. [3]Department of Paediatrics and Adolescent Medicine, Hong Kong Children's Hospital, Kowloon, Hong Kong. [4]Department of Paediatrics and Adolescent Medicine, The University of Hong Kong, Pokfulam, Hong Kong. [5]Department of Medicine, The University of Hong Kong, Pokfulam, Hong Kong. [6]Department of Obstetrics and Gynaecology, The Chinese University of Hong Kong, Shatin, Hong Kong. [7]Department of Medicine, Loma Linda University, Loma Linda, California. [8]Department of Pathology, Hong Kong Children's Hospital, Kowloon, Hong Kong. [9]Department of Orthopaedics and Traumatology, The Chinese University of Hong Kong, Shatin, Hong Kong. [10]Department of Medicine and Therapeutics, The Chinese University of Hong Kong, Shatin, Hong Kong. [11]School of Biomedical Sciences, The Chinese University of Hong Kong, Shatin, Hong Kong. [12]Institute of Translational Medicine, Faculty of Health Sciences, University of Macau, Taipa, Macau. [13]Division of Hematology/Oncology, Department of Pediatrics, The Seventh Affiliated Hospital, Sun Yat-Sen University, Shenzhen, China. [14]Hong Kong Hub of Paediatric Excellence, The Chinese University of Hong Kong, Shatin, Hong Kong.

H. Wang, K.Y.Y. Chan, C.K. Cheng, and M.H.L. Ng contributed equally to this article.

C.-k. Li, A.W.K. Leung, and K.T. Leung are the co-senior authors of this article.

**Corresponding Authors:** Kam Tong Leung, E-mail: ktleung@cuhk.edu.hk; Chi-kong Li, Hong Kong Children's Hospital, 1 Shing Cheong Road, Kowloon Bay, Kowloon, Hong Kong. Phone: 852-3513-3176; Fax: 852-2636-0020; E-mail: ckli@cuhk.edu.hk; and Alex Wing Kwan Leung, E-mail: alexwkleung@cuhk.edu.hk

Blood Cancer Discov 2022;3:516–35

**doi:** 10.1158/2643-3230.BCD-22-0011

high-risk or relapsed/refractory leukemias, showing that 14% of patients could receive matched targeted therapies (14).

Instead of relying solely on genomics, acquiring functional information through direct profiling of the drug response of patient biopsies to complement static genetic measurements has been an appealing option to endow increasingly precise treatments and identify more patients who would benefit from targeted therapies (15). In this regard, myriad studies have dictated the drug-sensitivity pattern of AML, with the majority being conducted in the adult arena. These investigations elucidated the pharmacogenomic landscapes of *de novo*, relapsed or refractory AML (16, 17), molecularly targeted drug combinations of selective effectiveness (18), new agents of clinical relevance (19, 20), and feasibility/benefits of applying drug screening–guided therapies in the clinics (21–24). In pediatric AML, specifically, screening with 7,389 compounds on cell lines and shortlisted validation on patient samples identified gemcitabine and cabazitaxel with broad antileukemia activities (25). In addition, chemogenomic profiling of 73 pediatric AML specimens revealed gene signatures associated with responses to cytotoxic agents (26). Nonetheless, a high-dimensional gene–drug clinical data set for pediatric AML is currently lacking. In this study, we formally established the first pediatric AML-specific drug response profile, discovered new therapeutic vulnerabilities through in-depth integrative analyses with genomic, transcriptomic, and medical parameters, and realized evidence-based functional precision medicine in children.

## RESULTS

### Study Overview

We developed a cohort of 52 children (median age: 9 years) diagnosed with AML ($n$ = 47; 90.4%), MDS ($n$ = 2; 3.8%), or MPAL ($n$ = 3; 5.8%). The clinical characteristics, including demographics, diagnostic information, pathologic values, risk assignments, treatments, responses, and outcomes, are presented in Supplementary Table S1, with detailed annotations of individual patients documented in Supplementary Table S2. Major parameters are consistent with those reported in collaborative studies of pediatric AML (3), indicating cohort representativeness. Extensive drug and genomic profiling were performed on 46 specimens collected at diagnosis and 15 at relapse (Supplementary Table S3). Depending on the cellularity/viability of biopsies and the quality of genomic material, drug profiling was executed on 61 specimens from 52 patients, targeted sequencing on 60 specimens from 52 patients, and RNA sequencing (RNA-seq) on 48 specimens from 42 patients. The resulting data sets were subsequently integrated to build the functional genomic landscape of pediatric AML. The overall study design and sample usage is depicted in Supplementary Fig. S1.

### Drug Response Profile of Pediatric AML

The optimal culture conditions for AML specimens were determined by testing the performance of different basal media intended to support primary hematopoietic cells *ex vivo*. Stromal coculture was not opted due to throughput issues (27). Instead, we adopted a defined cocktail of myeloid cytokines, including stem cell factor (SCF), fms-like tyrosine kinase receptor-3 ligand (Flt3-L), interleukin-3 (IL-3), and interleukin-6 (IL-6), to maintain the myeloblasts (19). The duration of culture was set to 72 hours, considering the drug action mechanisms and the turnaround time for clinical implementation (28). Of the media tested, only StemSpan H3000, selected for subsequent experiments, was able to maintain the number of postculture myeloblasts (Supplementary Fig. S2A). All conditions unavoidably triggered a modest level of apoptosis (Supplementary Fig. S2B) and mediated entrance into the cell cycle (Supplementary Fig. S2C). Differentiation of myeloblasts, by definition of morphology, was occasionally evidenced (Supplementary Fig. S2D). With this system, 61 of 66 specimens (92.4%) were able to proceed to drug testing, with the remaining being predominantly acute promyelocytic leukemia.

*Ex vivo* drug-sensitivity profiling was performed with a collection of 45 bioactive agents (39 targeted and 6 chemotherapeutics) selected based on their molecular targets, stages of clinical development, and relevance to hematologic malignancies (Supplementary Table S4). Data of 42 specimens from 39 patients with full drug testing (i.e., 45 drugs tested) were applied to create a global view of the drug response pattern in pediatric AML by plotting 1,890 area under curve (AUC) values into a clustered heat map (Fig. 1A; Supplementary Table S5). Unsupervised clustering of drug activities identified distinct sensitivity patterns. Cluster A comprises 7 highly active compounds (median $IC_{50}$ <70 nmol/L), including the proteasome inhibitors bortezomib, carfilzomib, and oprozomib, HDAC inhibitor panobinostat, survivin inhibitor YM155, HSP90 inhibitor elesclomol, and BCL-2 inhibitor navitoclax. Cluster B comprises 14 generally active compounds (median $IC_{50}$ <700 nmol/L), including the cytotoxic agents cytarabine, daunorubicin, fludarabine, and mitoxantrone, as well as inhibitors against BCL-2, HSP90, proteasome, and tyrosine kinases. Venetoclax, dasatinib, methotrexate, and sunitinib in clusters C and D exhibited bimodal activities, with extreme sensitivity in some cases and complete resistance in others. Cluster E comprises 12 generally inactive compounds (median $IC_{50}$ >800 nmol/L except LCL161) with sporadic responses. Cluster F comprises 8 essentially inactive compounds, notably including many approved drugs for adult AML such as decitabine, enasidenib, and ivosidenib. By comparing the median $IC_{50}$ values of individual drugs with their maximum serum concentrations ($C_{max}$; Supplementary Table S6), effective concentrations of 30 drugs could be achieved pharmacologically.

We analyzed the concordance of drug sensitivity with respect to drug family assignment by computing the activity correlation coefficients among individual agents. By plotting the data onto a clustered heat map (Supplementary Fig. S3A), the analysis revealed highly concordant activities among constituent members in the same drug class, as best exemplified by proteasome inhibitors, indicating the robustness of our drug screening platform. However, we also identified discordant activities among members in the same drug class, as in the cases for BCL-2, BCR-ABL, and FLT3 inhibitors (Supplementary Fig. S3B), possibly reflecting their inherent differences in target specificities (29, 30).

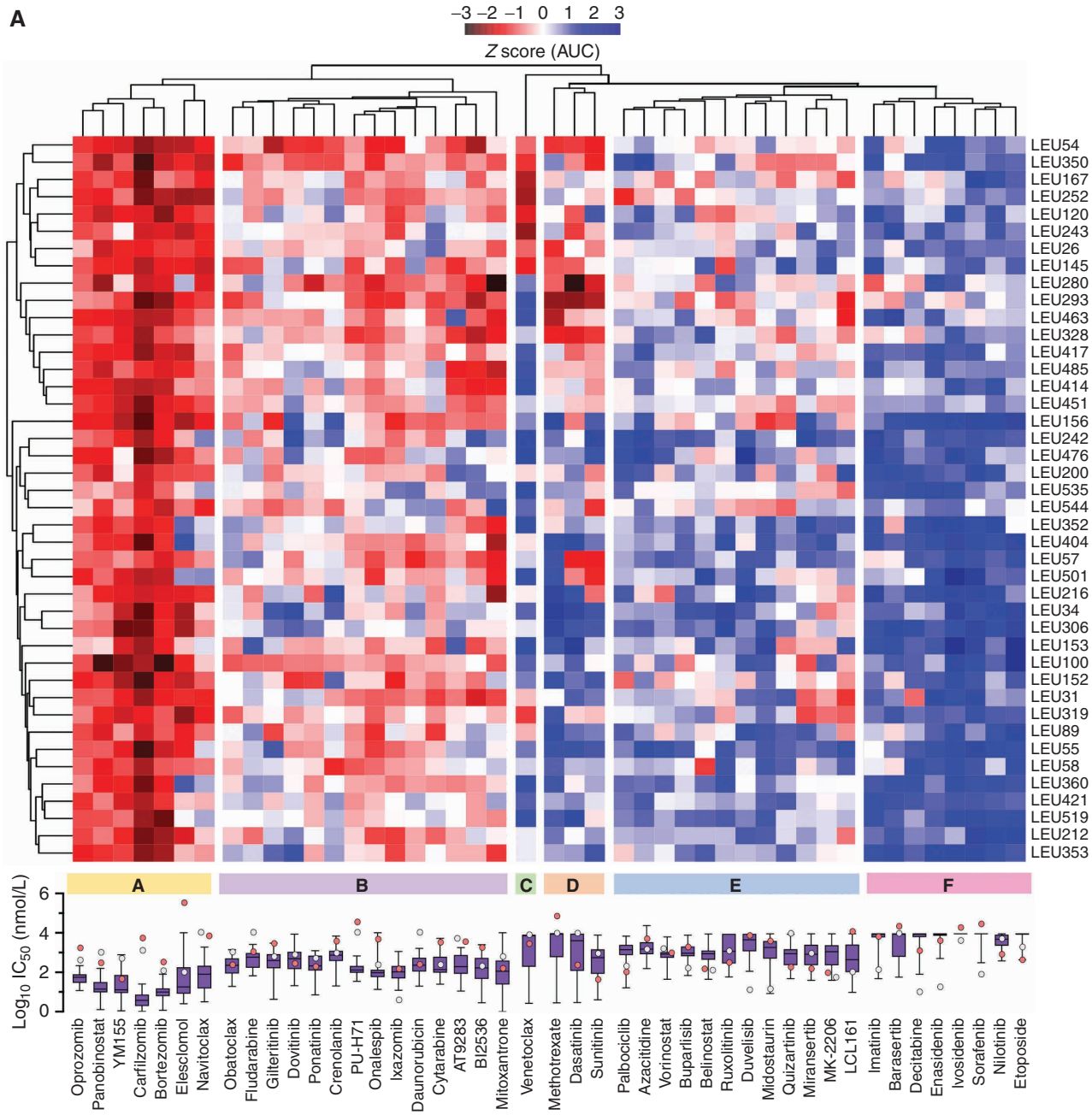


**Figure 1.** Drug response profile of pediatric AML. **A,** Heat map indicating the responses of 42 pediatric AML samples to 45 compounds represented by *Z*-score–transformed AUCs. Samples (rows) and drugs (columns) are ordered by unsupervised hierarchical clustering. Cluster A: highly active drugs with median $IC_{50}$ values <70 nmol/L. Cluster B: generally active drugs with median $IC_{50}$ values <700 nmol/L. Clusters C and D: drugs with bimodal activities. Cluster E: generally inactive drugs with sporadic exceptions. Cluster F: completely inactive drugs. The $IC_{50}$ distribution range for each compound is shown on the boxplot under the drug clusters, with median $IC_{50}$ values (white dots) and Cmax (red dots) depicted. (*continued on next page*)

Integration with patient pretreatment variables identified established and new clinical correlates of drug responses, such as resistance to cytotoxic agents for older children, and sensitivity to selected kinase inhibitors for patients with AML with MDS-related changes or adverse chromosomal anomalies (Fig. 1B). Analyses with posttreatment outcomes further demonstrated that resistance to cytarabine *ex vivo* was highly correlated with disease recurrence and death, with similar performance to risk stratification based on cytogenetics (Fig. 1C).

To compare the drug responses between diagnostic and relapsed AML, we performed PCA on the drug-sensitivity pattern of 32 diagnostic and 10 relapsed samples. Of these, matched paired samples were obtained from 6 patients. According to the distribution in the PCA plot, diagnostic and relapsed AML did not show discriminative differences in

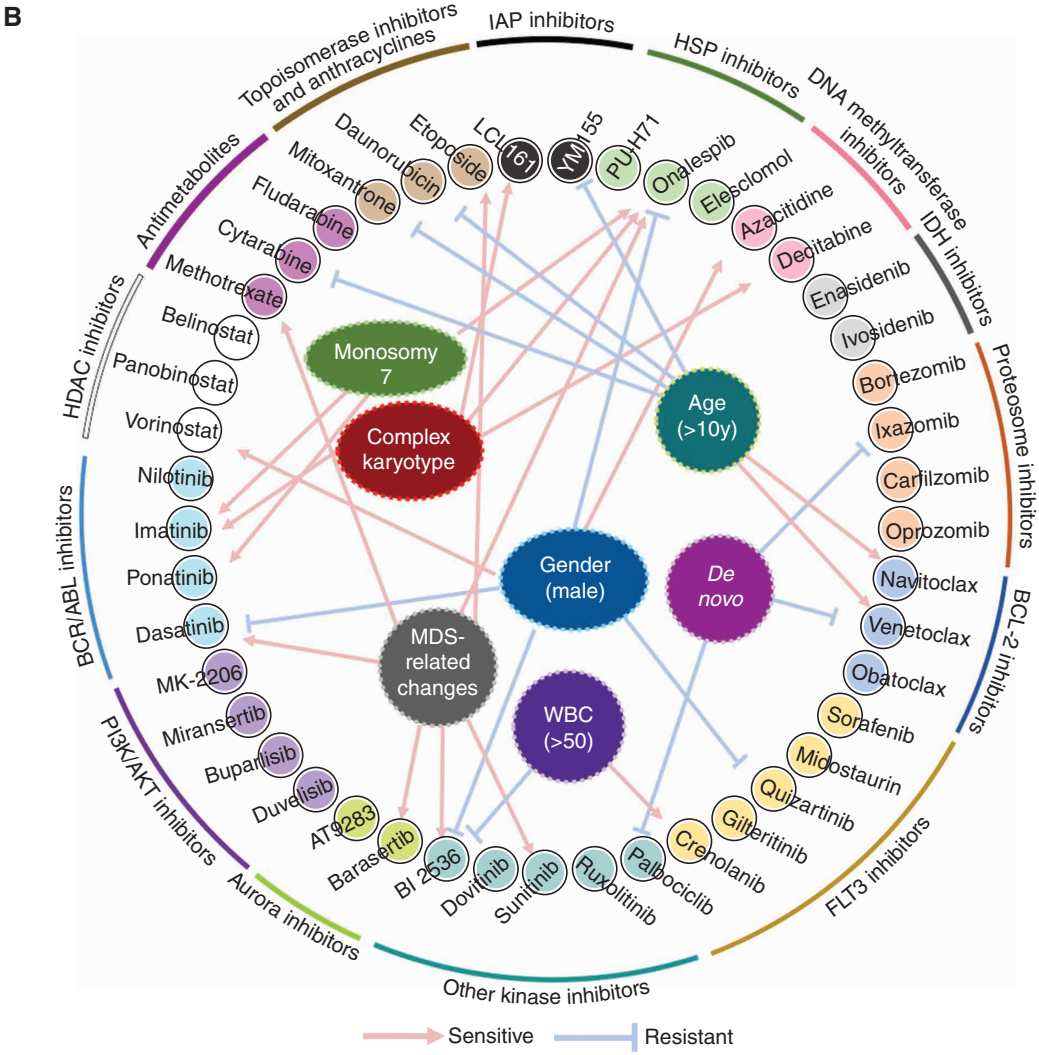


**Figure1.** ***(Continued)*** **B,** Correlation of pretreatment variables with drug sensitivity for the entire patient cohort ($n = 52$). Drugs are clustered on drug family. Significant associations ($P < 0.05$) are connected by arrows (sensitive) or edges (resistant). Drug sensitivity was assigned based on median AUCs. **C,** Forest plot showing the performance of cytogenetic risk group or *ex vivo* resistance to chemotherapeutics (defined by median AUCs) for prediction of clinical outcome. Patients ($n = 46$) with >12 months follow-up were included for analyses. Odds ratio of event (relapse or death), 95% confidence interval, and *P* values are shown. Statistics: **B**, two-tailed, unpaired Student *t* test; **C**, logistic regression.

their overall drug response profile (Supplementary Fig. S4A). Consistently, none of the drugs exhibited significant differences in activities between diagnostic and relapsed samples (Supplementary Fig. S4B), suggesting interindividual heterogeneity. We, therefore, attempted to capture any informative differences by comparing drug responses in pairwise diagnostic-relapsed samples. For two patients for whom full drug testing was performed in consecutive samples, we detected a more resistant signature at relapse than at diagnosis (Supplementary Fig. S4C). Dissection of specific drug responses in additional sample pairs revealed preferential resistance to cytarabine at relapse, corroborating clinical observations that patients with disease recurrence are generally less responsive to reinduction chemotherapy. Alternatively, YM155 consistently retained its effectiveness in relapsed samples (Supplementary Fig. S4D).

To look for specific differences in drug sensitivity between pediatric and adult AML, we performed functional drug screening using the same protocol in an adult cohort of 26 patients (median age: 53 years; clinical characteristics are shown in Supplementary Table S7). PCA did not show distinctive differences in the overall drug response pattern of pediatric versus adult AML (Fig. 2A). However, head-to-head comparisons of individual compounds demonstrated relative resistance of adult AML to fludarabine, daunorubicin, carfilzomib, ixazomib, belinostat, vorinostat, obatoclax, and dovitinib (Fig. 2B). In line with large-scale sequencing efforts (6, 12, 13), we detected profound age-specific differences in the mutational landscape between pediatric and adult AML (Fig. 2C), potentially explaining their dissimilar drug responses.

## *Ex Vivo* Drug Sensitivity Accurately Predicts *In Vivo* Responses

To strengthen the evidence for clinical implementation, we next validated whether the *ex vivo* drug testing system could fully capture *in vivo* activities. Complete drug-sensitivity profiling of 10 AML cell lines was performed to select the starting materials for animal modeling (Supplementary Table S8). Two drugs, namely, YM155 (survivin inhibitor) and venetoclax (BCL-2 inhibitor), exhibited bimodal activities. Considering their drug sensitivity and engraftment capability in immunodeficient mice, we opted OCI-AML3 (YM155 sensitive, $IC_{50}$: 23.1 nmol/L), MV4-11 (venetoclax sensitive, $IC_{50}$: 9.3 nmol/L), and CHRF-288-11 (YM155 and venetoclax resistant, $IC_{50}$: 3,977 nmol/L and 9,637 nmol/L) cells to establish xenografts (Supplementary Fig. S5A). Treatment of NOD/SCID mice grafted with luciferase-expressing OCI-AML3 cells with intraperitoneal YM155 substantially reduced bioluminescence signals reflecting systemic leukemic load by 85.5% at day 35 compared with those receiving vehicle control ($P = 0.0187$). Similarly, administration of oral venetoclax to mice grafted with MV4-11 cells also markedly reduced the leukemia burden by 92.6% at day 45 ($P = 0.0349$). In contrast, treatment of mice grafted with CHRF-288-11 cells with neither YM155 nor venetoclax diminished leukemia. Consistent with the leukemic load, single-agent YM155 and venetoclax significantly extended the survival of OCI-AML3–($P = 0.0084$) or MV4-11–transplanted animals ($P = 0.0173$) but not of those grafted with CHRF-288-11 cells (Supplementary Fig. S5B).

We further consolidated the predictive power of *ex vivo* drug responses in patient-derived xenografts (PDX). We chose venetoclax for modeling due to its prominent bimodal activities in pediatric AML. Based on the median $IC_{50}$ value (6,674 nmol/L) across the entire patient cohort, samples were classified into sensitive and resistant groups. A venetoclax-sensitive sample LEU350 ($IC_{50}$: 18.4 nmol/L) and a venetoclax-resistant sample LEU280 ($IC_{50}$: 7,183 nmol/L) were selected to generate xenografts (Fig. 3A). Concordant with activities *ex vivo*, venetoclax substantially reduced myeloblasts in the peripheral blood (PB) of NSG mice grafted with the venetoclax-sensitive sample ($P < 0.0001$). In contrast, for animals grafted with the venetoclax-resistant sample, no significant differences in the level of circulating myeloblasts between the vehicle and venetoclax groups were detected (Fig. 3B). Consistently, bone marrow (BM) sampling revealed a substantial drop in medullary leukemia in LEU350- (91.7% decrease) but not LEU280-transplanted mice following venetoclax treatments (Fig. 3C). Targeted sequencing of both primary samples revealed two founding clones before transplantation, and remained stable after leukemia engraftment (Fig. 3D).

We further performed cotitration experiments to explore the mode of interaction between targeted agents and chemotherapeutics. YM155 exhibited modest synergism with low-dose cytarabine but antagonism with daunorubicin in AML cell lines and patient samples in *vitro*. In contrast, venetoclax showed strong synergism with both cytarabine and daunorubicin (Supplementary Fig. S6A). In connection, combining YM155 with low-dose cytarabine delayed leukemia progression in OCI-AML3–transplanted mice compared with those receiving YM155 ($P = 0.0467$) or cytarabine alone ($P = 0.002$). Similarly, in MV4-11–transplanted mice, coadministration of venetoclax with cytarabine resulted in the most profound clearance of AML ($P < 0.05$; Supplementary Fig. S6B).

## Integration of Drug and Genomic Profiling Identifies New Therapeutic Vulnerabilities and Response Predictors

We performed targeted sequencing of a 141-human myeloid neoplasm-related gene panel (Supplementary Table S9). This panel enriches a library of commonly mutated genes and the most relevant variants in myeloid neoplasms listed in the Cancer Genome Atlas, Cancer Gene Census, and Catalogue of Somatic Mutations in Cancer (COSMIC). Of 52 pediatric patients with their first sample being analyzed, 45 (86.5%) carried ≥3 mutations, with 73 genetic alterations being recurrent. The complete variant list is shown in Supplementary Table S10. The genomic landscape was visualized by a mosaic plot with annotations of mutation types, pathogenicity, sample nature, cytogenetic risk groups, and events (Fig. 4A). The most frequent mutations were *KMT2C* (23.1%), *RELN* (19.2%), *FLT3* (17.3%), *JAK2* (15.4%), *KIT* (13.5%), and *NRAS* (13.5%). Consistent with the TARGET AML study (6), other common alterations in pediatric AML, such as *WT1* (11.5%), *CBL* (9.6%), and *KRAS* (7.7%), were also detected in our cohort. Mutations frequently found in adult AML (9, 10), including *DNMT3A*, *IDH1/2*, and *NPM1*, occurred rarely.

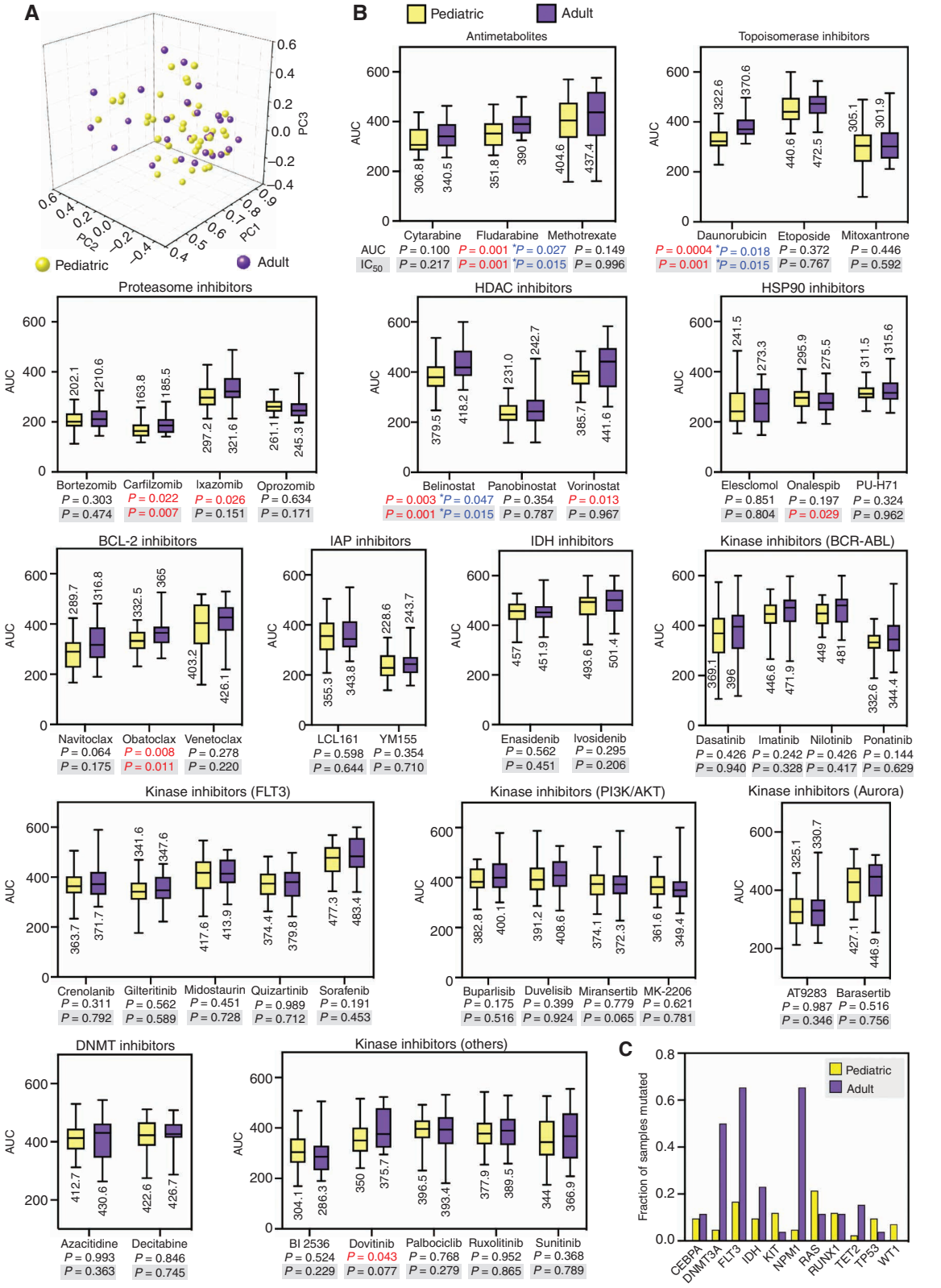


**Figure 2.** Drug-sensitivity profiles of pediatric and adult AML. **A,** PCA of the response parameter (i.e., AUC values of 45 drugs) in pediatric ($n = 42$) and adult AML ($n = 26$) samples. **B,** Boxplots showing the AUC distributions of individual drugs, ordered by drug classes. Statistics: two-tailed, unpaired Student *t* test. *P* values comparing both AUCs and $IC_{50}$ values are indicated. Statistically significant values are shown in red. Asterisks mark statistically significant differences after correction for multiple comparison by the Benjamini–Hochberg procedure, with *P* values after FDR correction shown in blue. **C,** Fraction of pediatric ($n = 52$) and adult ($n = 26$) samples with major genetic alterations detected by targeted sequencing.

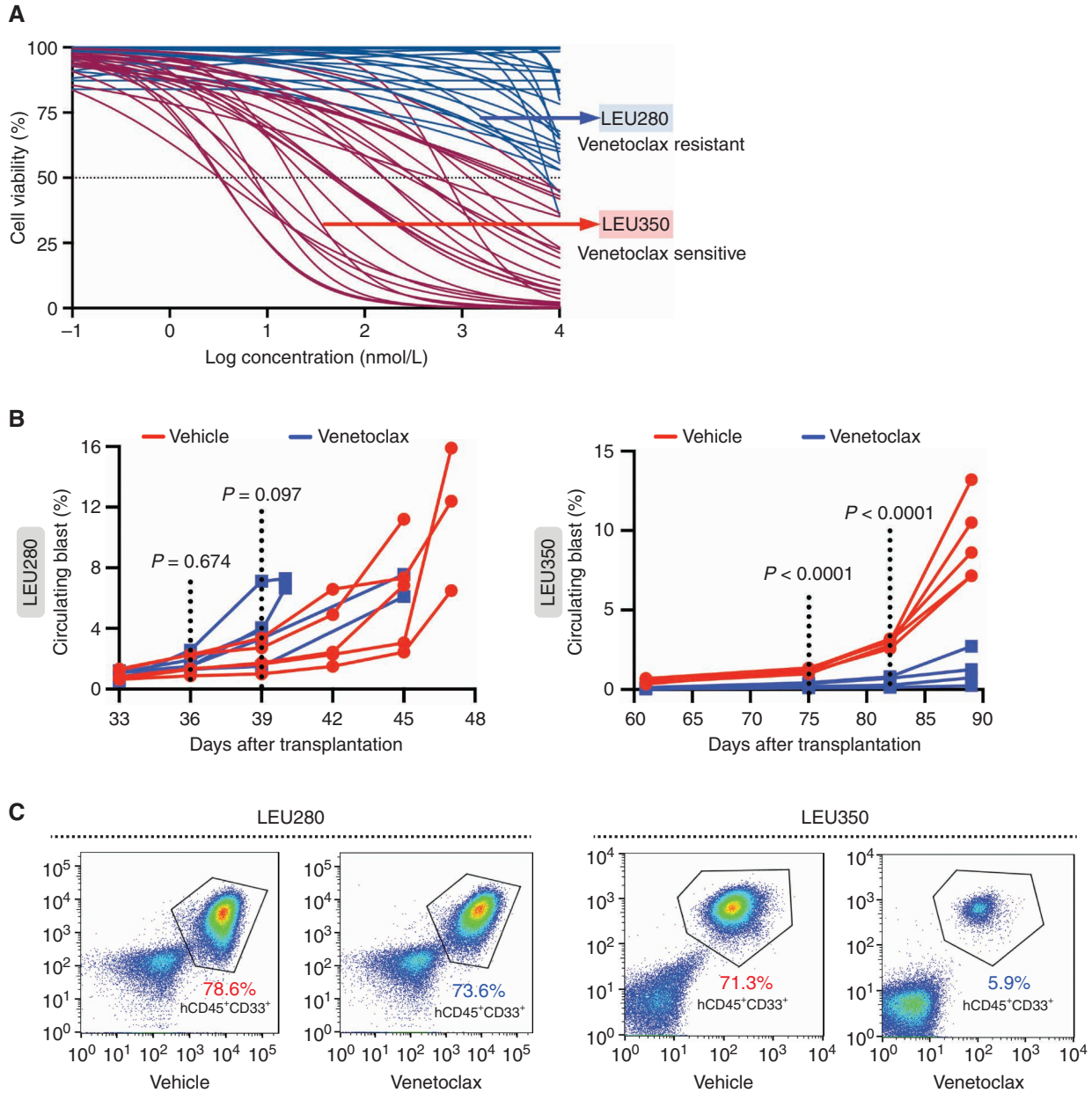


**Figure 3.** *Ex vivo* drug activities capture *in vivo* responses. **A,** Dose–response curves of venetoclax on primary myeloblasts from 54 pediatric AML samples (diagnosis, $n = 42$; relapse, $n = 12$). Samples exhibiting sensitivity (red curves) or resistance (blue curves) were classified with respect to the median $IC_{50}$ value (6,674 nmol/L) across the patient cohort. Arrows mark the samples selected for animal modeling. **B,** NSG mice were transplanted with myeloblasts derived from a venetoclax-resistant (LEU280) or a venetoclax-sensitive (LEU350) sample to generate PDXs. Animals (4–5 mice/group) were randomized to receive vehicle or oral venetoclax (100 mg/kg, once daily, 5 days/week for 2 weeks). Treatments commenced on day 3 after transplantation. Circulating leukemic blasts were monitored serially by flow-cytometric detection of human $CD45^+CD33^+CD19^-$ cells. Statistics: two-tailed, unpaired Student *t* test. *P* values are indicated. **C,** BM samples were collected on day 45 (LEU280) and day 89 (LEU350) posttransplantation for the enumeration of medullary leukemia. (*continued on next page*)

Associations between genetic mutations and drug sensitivity were mined by one-way ANOVA. The data set was first trained by two established gene–drug association (*FLT3*–crenolanib and *JAK2*–ruxolitinib; ref. 16) to determine the impact of variant allele frequency (VAF) and pathogenicity. The *FLT3*–crenolanib association appeared only with a pathogenicity filter and was retained at VAF of either 5% (16), 10% (31), or 20% (11), whereas the *JAK2*–ruxolitinib association was detected regardless of pathogenicity curation but lost at VAF cutoff of 20% (Supplementary Table S11). We, therefore, kept pathogenic and likely pathogenic variants (collectively referred to as pathogenic hereafter) with VAF >10% for downstream analyses. This algorithm retrieved 69 recurrent gene–drug associations, with 57 being novel (Supplementary Table S12). As depicted in a volcano plot (Fig. 4B), samples with *JAK2* and *FLT3* mutations exhibited sensitivity to the

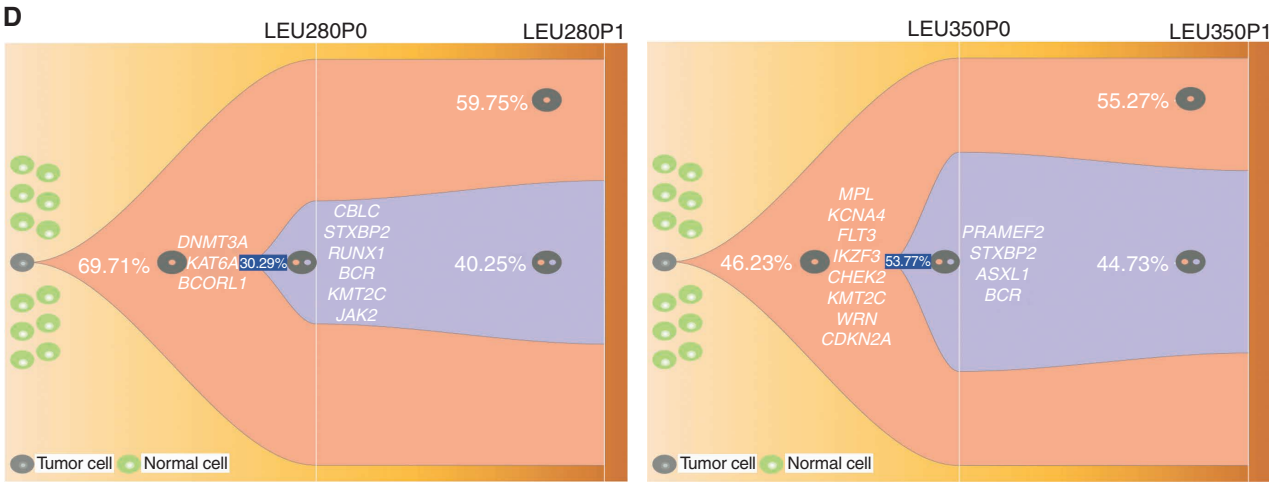


**Figure 3.** ***(Continued)*** **D,** Fish plots showing the evolution of subclonal architecture for samples LEU280 and LEU350 before (P0) and after (P1) leukemia engraftment in the BM of control NSG mice at the overt disease stage (i.e., day 45 for LEU280 and day 89 for LEU350).

JAK2 inhibitors ruxolitinib ($P = 0.04$) and AT9283 ($P = 0.03$), and the FLT3 inhibitor crenolanib ($P = 0.009$), respectively, consolidating the validity of this analysis. Of those novel gene–drug associations, we spotted samples harboring missense or nonsense mutations of lysine methyltransferase 2C (*KMT2C*), the most prevalent alteration in our cohort, showed significant associations with sensitivity to BCL-2 inhibitors ($P < 0.05$). Specifically, samples with pathogenic *KMT2C* variants were particularly sensitive to navitoclax or venetoclax, compared with those harboring benign variants or wild-type *KMT2C* ($P < 0.05$; Fig. 4C). Further integration with clinical outcome data revealed an exceedingly poor event-free survival rate for patients harboring mutant *KMT2C* ($P = 0.0114$), especially for those bearing variants defined as pathogenic (Fig. 4D), thereby successfully identifying a high-risk AML subtype that might benefit from targeted therapies.

We further conducted RNA-seq to identify the gene signatures underpinning the drug response. The counts per million mapped reads (CPM) values for the entire transcriptome of 48 sequenced samples are listed in Supplementary Table S13. Samples were first stratified into sensitive, intermediate, and resistant groups based on the distribution of AUCs (Fig. 5A). Among 45 drugs, 8 in cluster F demonstrated poor activities, and therefore 37 drugs were proceeded to analyses. Differentially expressed genes (DEG) between sensitive and resistant samples were then identified for each drug using FDR <0.05 and fold change >4 as the cutoffs, resulting in 1 to 820 DEGs for 36 drugs (Fig. 5B). Volcano plots of DEGs for venetoclax and YM155, for illustration, are shown in Fig. 5C. We convincingly detected significantly higher expression of *BCL2* (venetoclax target) in venetoclax-sensitive versus venetoclax-resistant samples (4.7-fold, $P < 0.0001$), indicating on-target activities. In contrast, we failed to detect *BIRC5*/survivin overexpression (YM155 target) in YM155-sensitive samples ($P = 0.374$), suggesting off-target activities. We further extended correlation analyses between DEGs and drug sensitivity to specimens with intermediate responses. A cutoff of Pearson $r$ value of >0.5 or < −0.5 was set to retain high-confidence predictors of drug sensitivity. We identified 98 and 91 DEGs with such properties for venetoclax and YM155, respectively (Fig. 5D). For venetoclax, most DEGs passing the cutoff criteria were negatively correlated with the $IC_{50}$ values. As a BCL-2–specific inhibitor, we concretely detected a strong correlation between venetoclax sensitivity and *BCL2* expression ($r = -0.639$, $P < 0.001$) but also hit, for instances, phosphodiesterase 7A (*PDE7A*; $r = -0.7511$, $P < 0.0001$) and zinc finger protein 114 (*ZNF114*; $r = -0.6572$, $P < 0.001$) with even better correlations. For YM155, most DEGs were positively correlated with AUCs. Again, its curated target survivin (*BIRC5*) was not correlated with drug sensitivity ($r = -0.1078$, $P = 0.4808$). Indeed, we identified other DEGs as strong predictors of YM155 activities, such as major histocompatibility

**Figure 4.** Integration of genomic alterations with drug sensitivity. **A,** Mosaic plot showing the mutational landscape of 52 pediatric patients with AML. The earliest specimen was included for analyses for individuals with consecutive sampling. Recurrent mutations occurring in ≥2 patients are shown and ranked by their frequencies in the cohort illustrated by the bar chart. Patients are annotated with clinical features and mutations with types. Asterisks mark pathogenic or likely pathogenic variants. **B,** Gene–drug associations represented by a volcano plot showing their significance and effects between wild-type and mutant samples. Pathogenic or likely pathogenic variants with VAF >10% were included for the analysis. A *P* value cutoff of 0.05 (horizontal line) was applied to detect statistically significant associations. A *Z* score cutoff of 0 (vertical line) defines relative drug sensitivity (red circles) and resistance (blue circles). The size of circles represents the number of patients harboring the mutations. Circles annotated with green and black texts denote known and novel associations, respectively. **C,** Box plots showing the activities of BCL-2 inhibitors in pediatric AML stratified by *KMT2C* mutation status: wild-type ($n = 29$–$35$), benign or likely benign mutants ($n = 8$), pathogenic or likely pathogenic mutants ($n = 3$–$4$). Median $IC_{50}$ values are shown. **D,** Kaplan–Meier estimates of 3-year event-free survival (period from diagnosis to first relapse or death from any cause) in patients with wild-type ($n = 40$), benign ($n = 8$), and pathogenic *KMT2C* ($n = 4$). Statistics: **B**, one-way ANOVA; **C**, two-tailed, unpaired Student *t* test with correction for multiple comparison by the Benjamini–Hochberg method; **D**, log-rank test. *, $P < 0.05$; **, $P < 0.01$.

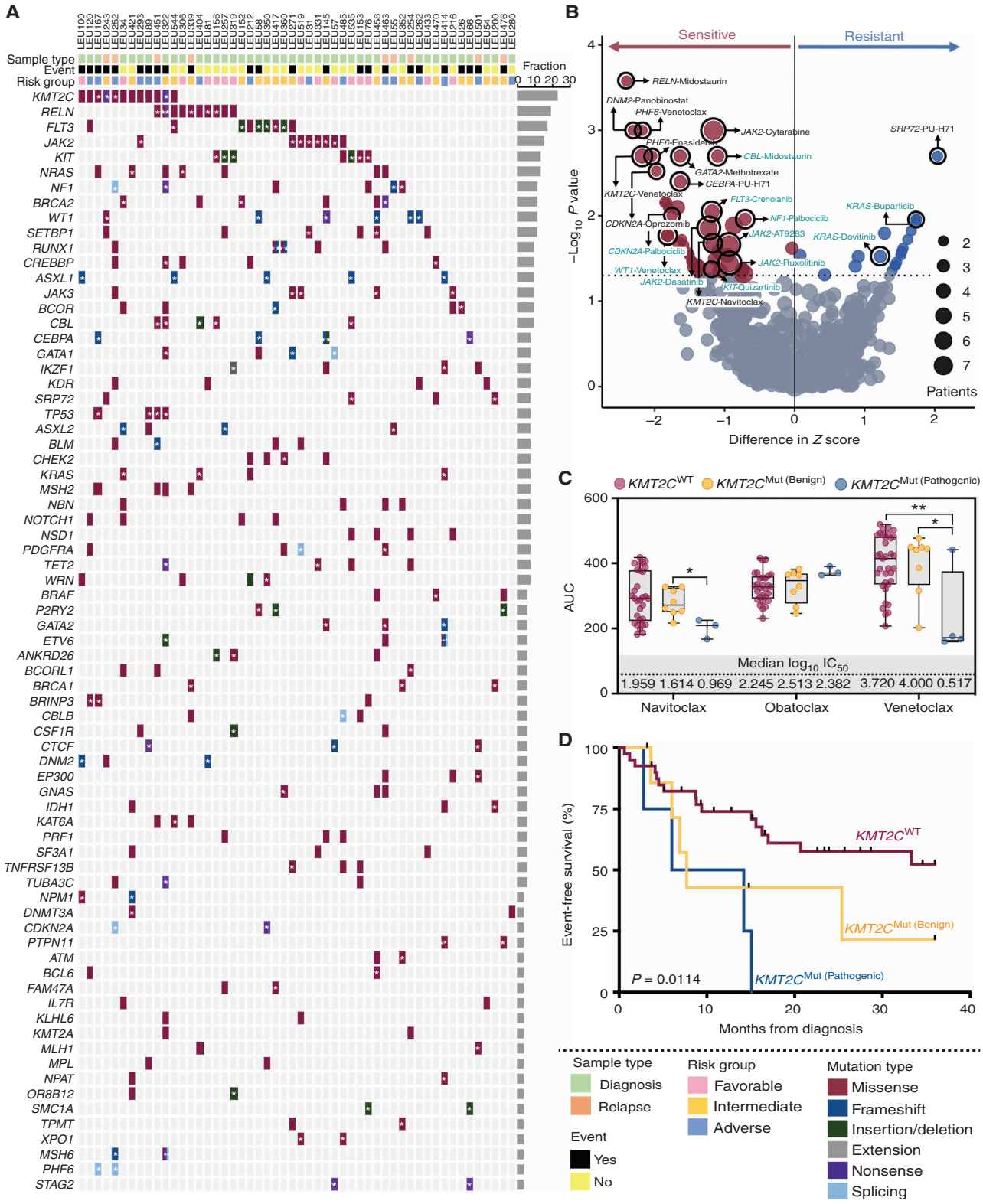
A
Sample type
Event
Risk group
Fraction
0 10 20 30
KMT2C
RELN
FLT3
JAK2
KIT
NRAS
NF1
BRCA2
WT1
SETBP1
RUNX1
CREBBP
ASXL1
JAK3
BCOR
CBL
CEBPA
GATA1
IKZF1
KDR
SRP72
TP53
ASXL2
BLM
CHEK2
KRAS
MSH2
NBN
NOTCH1
NSD1
PDGFRA
TET2
WRN
BRAF
P2RY2
GATA2
ETV6
ANKRD26
BCORL1
BRCA1
BRINP3
CBLB
CSF1R
CTCF
DNM2
EP300
GNAS
IDH1
KAT6A
PRF1
SF3A1
TNFRSF13B
TUBA3C
NPM1
DNMT3A
CDKN2A
PTPN11
ATM
BCL6
FAM47A
IL7R
KLHL6
KMT2A
MLH1
MPL
NPAT
OR8B12
SMC1A
TPMT
XPO1
MSH6
PHF6
STAG2
B
Sensitive
Resistant
RELN-Midostaurin
DNM2-Panobinostat
PHF6-Venetoclax
JAK2-Cytarabine
SRP72-PU-H71
PHF6-Enasidenib
CBL-Midostaurin
GATA2-Methotrexate
CEBPA-PU-H71
KMT2C-Venetoclax
FLT3-Crenolanib
KRAS-Buparlisib
CDKN2A-Oprozomib
NF1-Palbociclib
JAK2-AT9283
KRAS-Dovitinib
CDKN2A-Palbociclib
JAK2-Ruxolitinib
WT1-Venetoclax
JAK2-Dasatinib
KIT-Quizartinib
KMT2C-Navitoclax
−Log10 P value
Difference in Z score
Patients
C
KMT2CWT
KMT2CMut (Benign)
KMT2CMut (Pathogenic)
AUC
Median log10 IC50
1.959 1.614 0.969 2.245 2.513 2.382 3.720 4.000 0.517
Navitoclax
Obatoclax
Venetoclax
D
Event-free survival (%)
KMT2CWT
KMT2CMut (Benign)
KMT2CMut (Pathogenic)
P = 0.0114
Months from diagnosis
Sample type
Diagnosis
Relapse
Event
Yes
No
Risk group
Favorable
Intermediate
Adverse
Mutation type
Missense
Frameshift
Insertion/deletion
Extension
Nonsense
Splicing

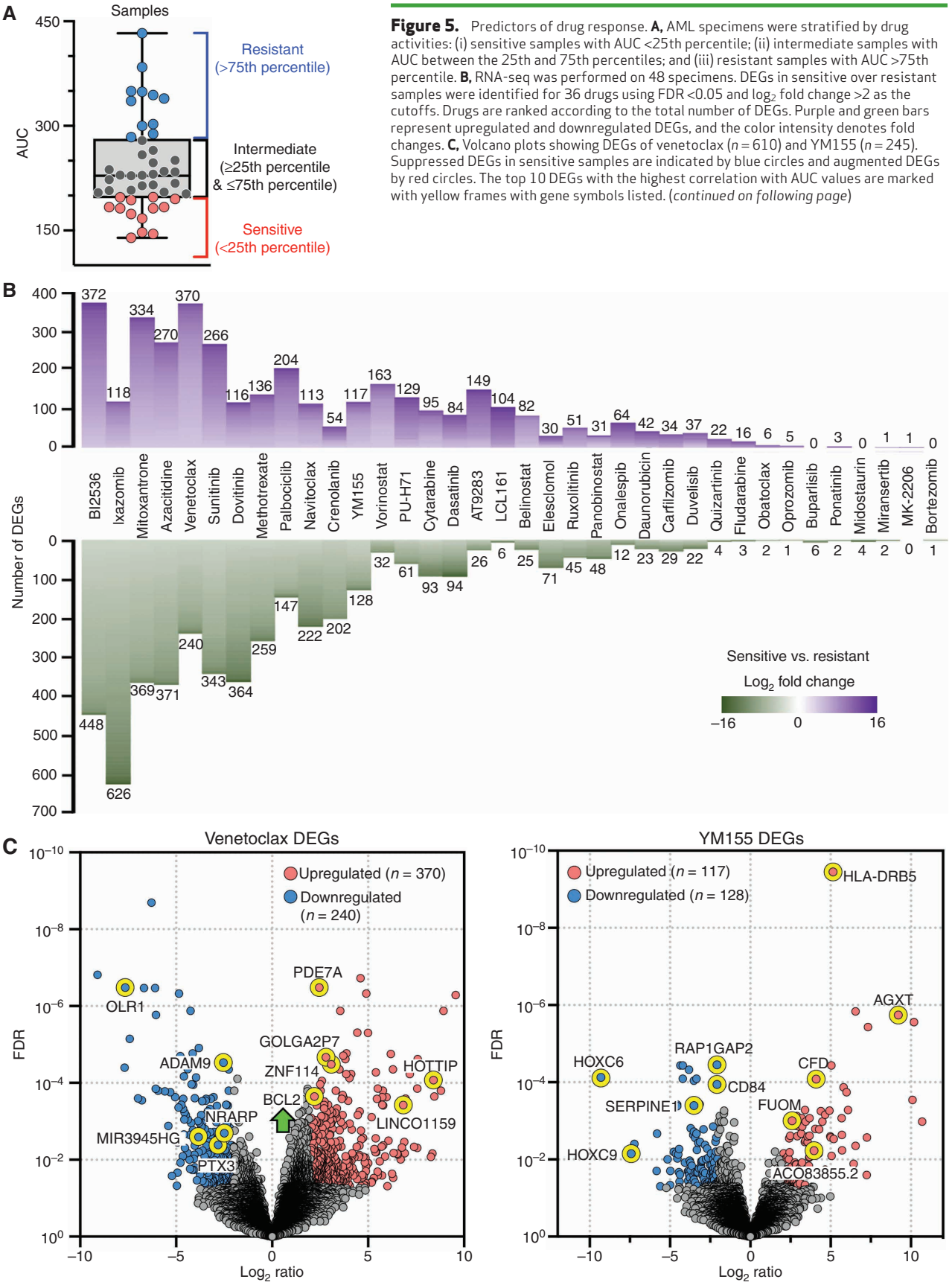


**Figure 5.** Predictors of drug response. **A,** AML specimens were stratified by drug activities: (i) sensitive samples with AUC <25th percentile; (ii) intermediate samples with AUC between the 25th and 75th percentiles; and (iii) resistant samples with AUC >75th percentile. **B,** RNA-seq was performed on 48 specimens. DEGs in sensitive over resistant samples were identified for 36 drugs using FDR <0.05 and $\log_2$ fold change >2 as the cutoffs. Drugs are ranked according to the total number of DEGs. Purple and green bars represent upregulated and downregulated DEGs, and the color intensity denotes fold changes. **C,** Volcano plots showing DEGs of venetoclax ($n = 610$) and YM155 ($n = 245$). Suppressed DEGs in sensitive samples are indicated by blue circles and augmented DEGs by red circles. The top 10 DEGs with the highest correlation with AUC values are marked with yellow frames with gene symbols listed. (*continued on following page*)

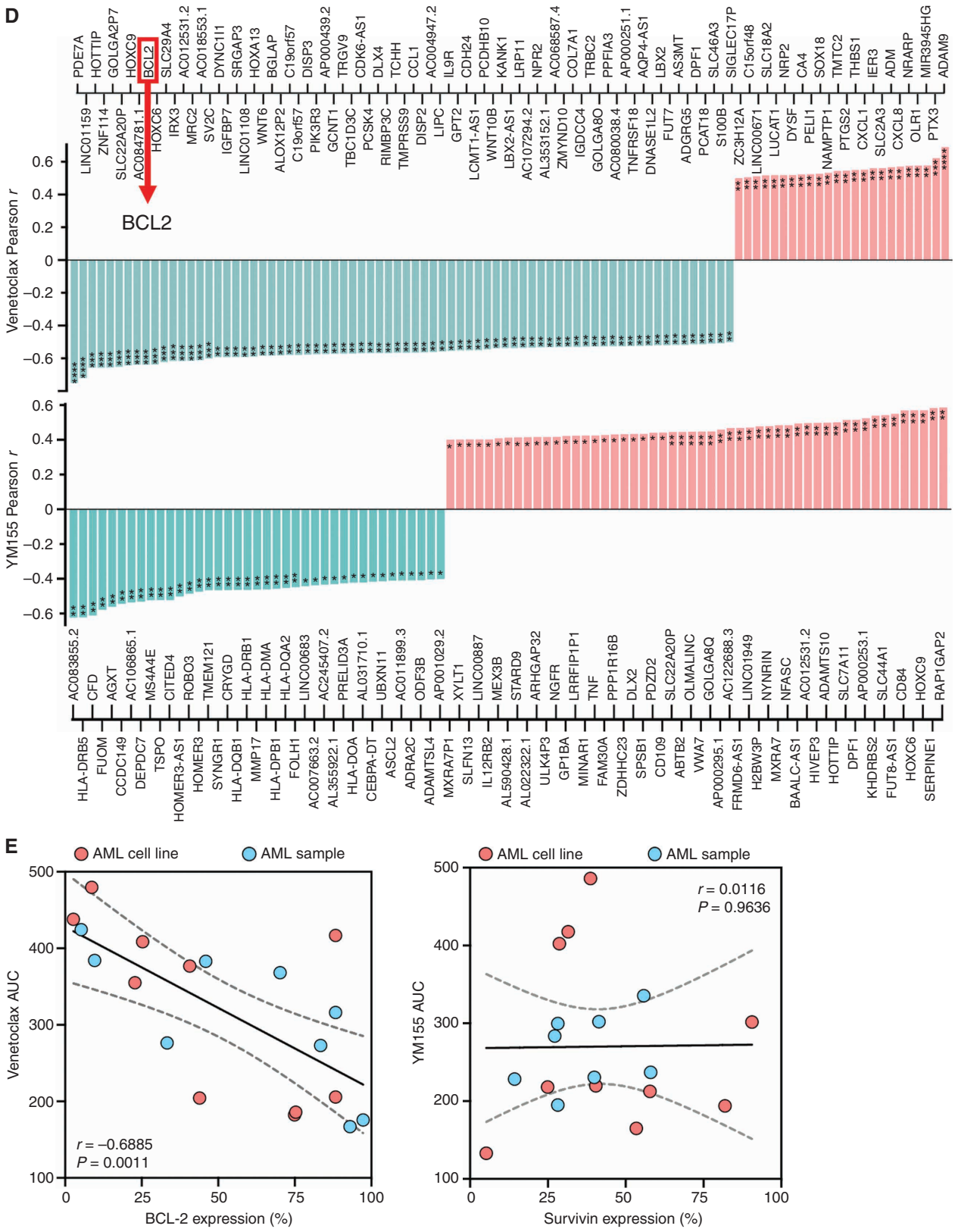


**Figure 5.** ***(Continued)*** **D,** Correlation analyses between DEG (CPM) and drug sensitivity (AUC). DEGs of venetoclax ($n = 98$) and YM155 ($n = 91$) with correlation coefficients of < –0.5 or >0.5 are shown and ranked according to the magnitude of correlation. Positively correlated DEGs are indicated by pink bars, and negatively correlated DEGs by green bars. Arrow indicates the venetoclax target BCL-2. **E,** Intracellular BCL-2 and survivin expression in AML cell lines ($n = 10$) and samples ($n = 8$–9) was measured by flow cytometry and correlated with venetoclax and YM155 sensitivity, respectively. Statistics: **B**, **C**, DESeq2; **D**, **E**, Pearson correlation. *, $P < 0.05$; **, $P < 0.01$; ***, $P < 0.001$; ****, $P < 0.0001$.

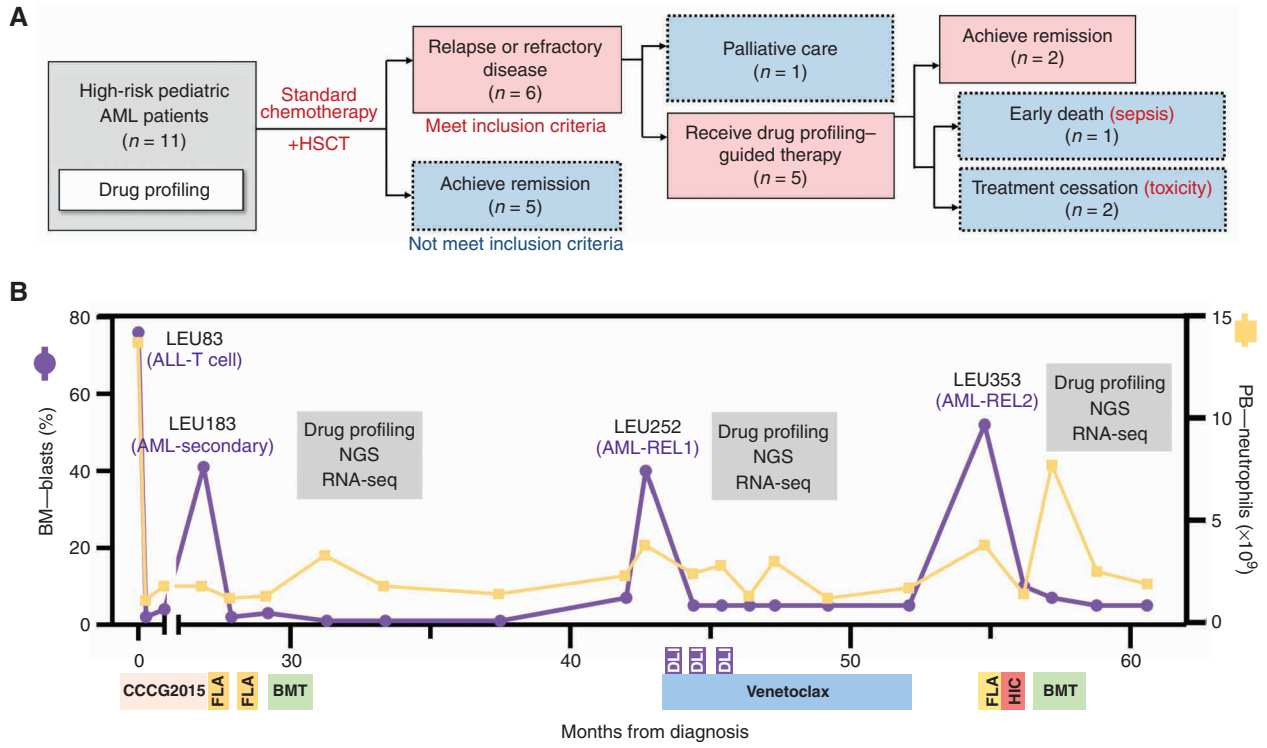


**Figure 6.** Precision medicine for high-risk pediatric AML. **A,** Flowchart showing the workflow of this pilot clinical trial, including patient numbers at each stage and reasons for dropping out of the study. **B,** Clinical progression of a child with relapsed AML receiving drug profiling-guided treatment. The disease course, treatment landscape, and laboratory investigations are depicted. (*continued on following page*)

complex class II DR beta 5 (*HLA-DRB5*; $r = -0.6222$, $P < 0.01$) and complement factor D (*CFD*; $r = -0.6114$, $P < 0.01$). The functional significance of these DEGs remains largely unknown and warrants further investigation. By intracellular flow cytometry, we confirmed a strong correlation of BCL-2 expression with venetoclax sensitivity but not survivin expression with YM155 sensitivity at the protein level (Fig. 5E), therefore validating the usefulness of this stepwise approach to discover new predictors of drug response.

Further mining of RNA-seq data detected 14 recurrent, in-frame gene fusions in 27 of 42 patients (64.3%). Concordant with recent reports (6, 32), the most prevalent fusions in our cohort were *RUNX1–RUNX1T1* (16.7%), *KMT2A* (16.7%), and *NUP98* (11.9%) rearrangements (Supplementary Fig. S7A). Correspondingly, we identified significant associations with their preferential sensitivity to YM155/azacitidine ($P < 0.05$), venetoclax ($P = 0.024$), and nilotinib/mitoxantrone ($P < 0.05$), respectively (Supplementary Fig. S7B).

## Precision Medicine for High-Risk Pediatric AML

Since the study inception, we integrated the platforms developed to test the feasibility of implementing precision medicine for pediatric AML in the clinical setting. A flowchart showing our decision-making algorithm is shown in Fig. 6A. Drug profiling was performed prospectively and reported to the tumor board for 11 patients who were deemed high risk. Standard treatments (i.e., chemotherapy plus HSCT) were offered, but 6 patients developed relapsed or refractory diseases, fulfilling the inclusion criteria for precision medicine. Of these subjects, one opted palliative care by family decision and 5 had received drug profiling-guided therapy. Three patients were not eligible to evaluate treatment response due to early death or drug toxicity (one patient died due to progressive disease within a week after targeted therapy whereas two patients developed therapy-related leukoencephalopathy, acute confusion, slurred speech, or nausea leading to treatment cessation). Here, we present in detail 2 cases who had achieved disease remission following adoption of functional precision medicine. The full disease course, treatment landscape, pathologic findings, and laboratory investigations are presented in Supplementary Tables S14 and S15.

A 14-year-old boy was initially diagnosed with T-cell ALL with a hypodiploid karyotype (Fig. 6B). He was treated with the Chinese Children Cancer Group (CCCG) ALL protocol (33) under the intermediate-risk arm and achieved remission. During maintenance, blasts emerged with a lineage switch to myeloid phenotypes and acquired complex cytogenetics likely representing endoduplication of the hypodiploid clone, suggestive of secondary AML (sample LEU183). He then received two courses of fludarabine–cytarabine (FLA, a standard chemotherapy-based regimen for relapsed AML) and matched sibling donor HSCT, and achieved remission. A recurrent BM relapse developed 1 year after HSCT (sample LEU252). We, therefore, performed full drug profiling on his myeloblasts

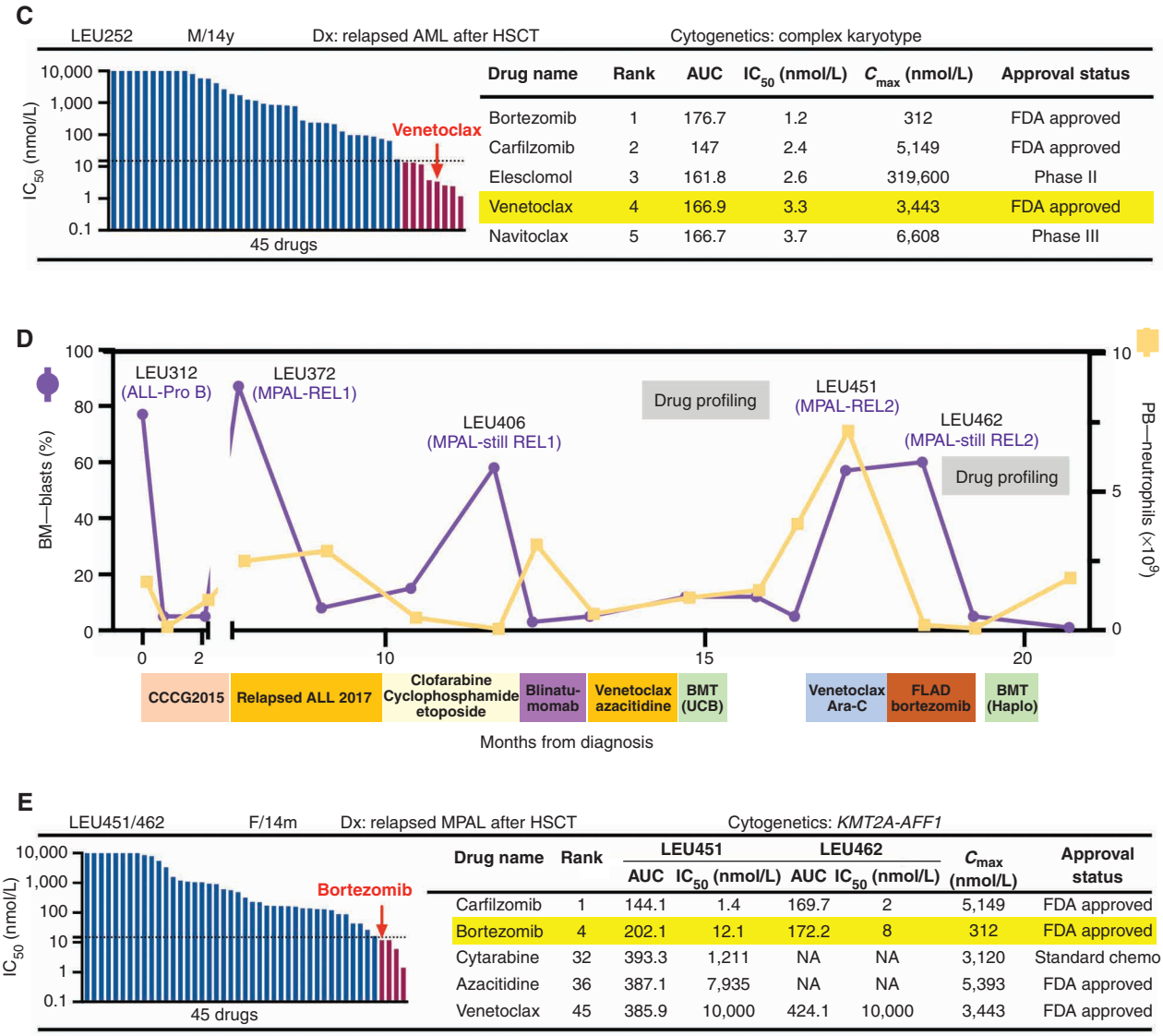


**Figure 6.** ***(Continued)*** **C,** Drug profiling results at first AML relapse. The bar chart shows the activities of 45 screened drugs ranked in descending $IC_{50}$ values. The horizontal line at 15 nmol/L was arbitrarily set to indicate highly active drugs. The table shows the top-hit drugs annotated with respective $IC_{50}$ values, AUC, $C_{max}$, and FDA-approval status. The drug recommended by the tumor board is indicated by an arrow in the bar chart and highlighted in yellow in the table. **D** and **E,** Clinical progression, drug testing results, and therapy recommendation for another case with relapsed MPAL. Abbreviations: BMT, bone marrow transplantation; DLI, donor leukocyte infusion; FLA, fludarabine and cytarabine; FLAD, fludarabine, cytarabine, and daunorubicin; HIC, high-intensity consolidation.

and identified exceptional sensitivities to BCL-2 inhibitors (Fig. 6C). Venetoclax, instead of universally active agents, was recommended by the tumor board given its reported safety and efficacy in relapsed/refractory pediatric AML (34) as well as local accessibility. In an off-label, compassionate and outpatient setting, the patient received venetoclax at 100 mg/m$^2$ and then stepped up to 400 mg/m$^2$ daily for 9 months concomitant with donor lymphocyte infusions, resulting in a rapid and sustained clearance of blasts, demonstrating a match between *ex vivo* and *in vivo* responses. However, a frank relapse developed 2 months after cessation of venetoclax therapy (sample LEU353). We, therefore, performed another drug profiling for the patient but revealed the acquisition of pan-resistance to 34 drugs in the panel, especially venetoclax (Supplementary Fig. S8A). Further treatment with FLA and high-intensity consolidation resulted in a considerable drop in blasts but failed to achieve complete remission, consistent with its chemoresistance nature. The patient further received haploidentical HSCT and was brought into remission. Complementary genomic profiling was performed on serial samples to dictate the disease evolution and dynamics of drug responses. Targeted resequencing revealed the existence of a diverse subclonal architecture already at diagnosis (LEU183), with 9 detectable genomic lesions (Supplementary Fig. S8B). Two additional mutations appeared at first relapse (LEU252) and remained stable at second relapse (LEU353) after venetoclax monotherapy, excluding further clonal evolution. RNA-seq revealed apparent transcriptomic changes throughout

the disease course (Supplementary Fig. S8C). Convincingly, the 98-gene signature (see Fig. 5D) was, in general, predictive of venetoclax resistance at the second relapse (Supplementary Fig. S8D), therefore capturing specific alterations in drug responses.

A 14-month-old girl was diagnosed with Pro-B ALL harboring the high-risk *KMT2A–AFF1* t(4;11) chromosomal translocation (Fig. 6D). She was treated under the CCCG ALL protocol and achieved molecular remission. Unfortunately, an early relapse developed with a mixed lymphoid/myeloid phenotype (MPAL) and was managed with the Relapsed ALL protocol and then salvage chemotherapy but failed to attain complete remission. Her refractory disease was subsequently resolved by blinatumomab, followed by venetoclax/azacitidine maintenance and umbilical cord blood HSCT. A second relapse developed at 3 months after transplantation (sample LEU451) and was immediately given a course of venetoclax in combination with high-dose cytarabine. However, our drug profiling results revealed resistance to both agents (Fig. 6E). In agreement with these findings, no clinical response was witnessed (sample LEU462), and the clinicians, therefore, decided to stop the therapy. We then performed a second drug profiling and revealed reproducible sensitivity to bortezomib. As recommended by the tumor board, the patient received bortezomib at 1.3 mg/m$^2$ together with fludarabine, cytarabine, and daunorubicin (FLAD), achieved a third remission, and successfully bridged to a haploidentical HSCT.

## DISCUSSION

This study has nurtured the first functional genomic landscape of pediatric AML. Based on comprehensive drug-sensitivity profiling and systematic integration with genomic, transcriptomic, and clinical parameters, we deposited valuable data sets that could be leveraged to discover new therapeutic vulnerabilities, identify predictors of drug response, and deconvolute the mechanisms of drug resistance. Importantly, our intent is to adopt the platform to inform personalized therapies for patients who exhaust available treatments, thereby endowing a major impact on the future trial design to realize the importance of precision medicine.

To date, the drug-sensitivity pattern of AML has been predominantly studied in adults (16–20). By profiling the response of myeloblasts from children to a clinically relevant drug panel through an optimized *ex vivo* culture system, we showed that several approved targeted agents and investigational drugs, including bortezomib, carfilzomib, oprozomib, elesclomol, panobinostat, navitoclax, and YM155, are more potent than chemotherapeutics at clinically achievable concentrations. Although their effectiveness in pediatric AML remains to be established (35), our data delivered a wealth of opportunistic drug candidates that deserve to be prioritized in upcoming clinical trials. Notably, new agents approved for adult AML, such as midostaurin, ivosidenib, enasidenib, and decitabine, were essentially futile in their pediatric counterpart, therefore capturing the inherent differences in the prevalence of age-specific lesions at the functional level. Indeed, we formally compared the drug-sensitivity profile between pediatric and adult AML and demonstrated a more resistant nature of the latter to a number of cytotoxic and targeted agents, elucidating that AML of pediatric and adult origins are not only genetically and biologically different (6, 7), but are also distinct for drug responses. Through integration with clinical data, we further identified the association of patient-centric parameters, including age at diagnosis, cytogenetics, and disease stages, with drug susceptibility. Importantly, resistance to cytotoxic agents *ex vivo*, particularly cytarabine, was predictive of dismal outcomes, highlighting its potential value to be adopted for informing risk assignment. Though informative, the current drug testing system could have biased against agents requiring successive cell division cycles or provoking myeloblast differentiation given the short culture time and the choice of readout. Concurrent flow-cytometric assessment of differentiation markers at endpoints would avoid such underestimation of drug activities, especially for epigenetic agents (36). The inclusion of stromal feeders to better mimic the BM microenvironment is also an option for simulation of *in vivo* drug responses (22) but apparently will have an expense on throughput and ease of clinical implementation. Nevertheless, through animal modeling, we have provided compelling evidence showing the robustness of our drug testing platform in the prediction of *in vivo* responses, as exemplified by two targeted agents, venetoclax and YM155, exhibiting bimodal activities in pediatric AML. Whether the results could be generalized to other drugs would have to be further evaluated. In addition to single-agent activities, our system could also detect synergism of drug combinations, collectively providing a strong foundation for clinical inception.

By extended genomic profiling of pediatric AML specimens, we detected frequent alterations of *FLT3*, *JAK2*, *KIT*, *RAS*, and *WT1*, whereas mutations commonly found in adult AML, including *DNMT3A, IDH1/2*, and *NPM1*, were virtually absent, consistent with the reported molecular landscapes (6, 37). Taking the impact of variant pathogenicity and allele frequency into account, we integrated genomic findings with drug profiling data, revealing known gene–drug associations such as *FLT3*–crenolanib and *JAK2*–ruxolitinib. Convincingly, we also identified myriad novel associations of prognostic relevance and therapeutic implications. For example, mutation of *KMT2C*, also known as *MLL3*, was the most prevalent genomic lesion detected in our cohort. It is a tumor suppressor gene initially identified in adult AML (38) and recently also in children (39) where mutant *KMT2C* is linked to chemoresistance. By recalling the clinical outcome data, we showed that children harboring pathogenic *KMT2C* variants had extremely poor survival. Noteworthy, patients bearing so-called benign *KMT2C* variants still underperformed, pointing toward in-depth studies to redefine their impact in this disease context. Importantly, mining the drug profiling data revealed exceptional sensitivity of pathogenic *KMT2C* mutants to BCL-2 inhibitors. Therefore, with this algorithm, we could identify prognostically relevant alterations with new therapeutic vulnerabilities. The same is also true for common chimeric gene fusions in pediatric AML (6, 32), where previously unrecognized susceptibilities to targeted agents were identified for cases with favorable-risk *RUNX1–RUNX1T1*, intermediate-risk *KMT2A*, and adverse-risk *NUP98* rearrangements. However,

some gene–drug associations, particularly with comutations (16), might have been missing due to the limited size of our cohort and the targeted sequencing approach, implying that constant efforts through collaborative studies to extend the functional genomic landscape of this rare leukemia are required to definitively establish the correlations and yield new information. It is also likely that most of the drug dependencies are attributed to nongenomic causes and yet to be deduced.

We further performed transcriptome profiling to look for predictors of drug response and successfully retrieved DEGs for most of the agents in the panel. Applying correlation analyses ultimately yielded 36 high-confidence gene lists. Illustrated by venetoclax, we identified a 98-gene signature that could reflect its activity in pediatric AML. Convincingly, *BCL2* (venetoclax target) was on the list with a strong correlation between gene expression and drug sensitivity, indicating on-target activity. We also hit *PDE7A* and *ZNF114* with sound predictive values; therefore, these might contribute to the ever-expanding mechanisms underlying venetoclax response (40). Intriguingly, we failed to detect *BIRC5*/survivin overexpression (YM155 target) in YM155-sensitive samples, suggesting off-target activity (41). The top-ranked candidates in the 91-gene signature such as *HLA-DRB5* and *CFD* might indeed represent the true targets that remain to be elucidated by gene knockout studies. Therefore, the integration of transcriptomic and drug profiling data could not only identify response biomarkers that is particularly important for paucicellular specimens where drug testing remains inapplicable but also potentially uncover the mechanisms of drug resistance through further gene ontology and functional analyses.

Currently, most precision oncology initiatives focus on genomics, but this approach suffers from numerous practical hurdles. First, the turnaround time for molecular profiling is comparatively long, endowing the risk for delayed treatment. Second, genomic-based medicine requires highly experienced bioinformaticians for downstream analyses, limiting its generalization. Third, many of the genomic lesions, especially in pediatric AML, are not actionable, suggesting that only a minority of patients could benefit from matched targeted therapy (14). Direct profiling of drug sensitivity using a simplified methodology is, therefore, an attractive option to widen the applicability of precision medicine. In adults with advanced hematologic malignancies, harnessing such a functional approach to tailor individualized regimes has resulted in improved clinical outcomes (21–24). To this end, we adopted drug screening–guided treatment for 5 children with relapsed diseases who failed successive salvage therapies. Encouragingly, 2 evaluable patients achieved remission and bridged to curative HSCT. Noteworthy, venetoclax was given to both patients whose drug profiling showed opposing sensitivity that was fully reflected by subsequent clinical responses. These observations are in line with a phase I, dose-escalation study of venetoclax showing a 70% response rate in children with relapsed or refractory AML (34). Therefore, we propose incorporating drug profiling into upcoming clinical trials to determine its predictive potential and prioritize patients who will most probably benefit to receive the intervention. In addition, our analyses in serial samples revealed dynamic changes in drug responses and genomic/transcriptomic landscapes. Therefore, performing integrative drug and genomic profiling for a given patient in a continuous process will be the key to empowering precision medicine. However, adopting such nonstandard tactic for patient management, especially in children, would require expertise from the tumor board to prioritize hits for recommendation, taking careful consideration of potential toxicity, pediatric experience of particular agents, and drug cost. Finally, the real benefits of this approach would have to be further investigated in randomized studies.

## METHODS

### Specimens, Cells, and Cultures

All specimens were collected with parental written informed consent following the Declaration of Helsinki. The study was approved by the CUHK-NTEC and HKCH Ethics Committee. For children with myeloid malignancies, standard diagnostic workups were performed, including immunophenotyping, cytology, cytochemistry, and cytogenetics. Entities of cytogenetic/genetic anomalies and MDS-related changes were defined according to WHO guidelines (42) and risk-stratified with a pediatric algorithm (43). Biopsies were originated from BM except 2 cases from PB and 1 from ascitic fluid. Investigations were mostly performed with cryopreserved specimens ($n$ = 40; 65.6%), with the remaining being fresh ($n$ = 21). Mononuclear cells were recovered by Ficoll-Paque Plus (GE Healthcare). The purities of myeloblasts (median: 74.1%) were characterized by staining with CD33-BV421, CD34-PE-Cy7 (BD Biosciences), and CD45-APC (Beckman Coulter), followed by acquisition with a flow cytometer (LSRFortessa). FACS data were analyzed with FlowJo (TreeStar). Myeloblasts were maintained in StemSpan H3000 medium (Stem Cell Technologies) with SCF (50 ng/mL), Flt3-L (50 ng/mL), IL-3 (10 ng/mL), and IL-6 (10 ng/mL) (Miltenyi Biotec). Cell proliferation was determined by Trypan blue exclusion. Cell-cycle distribution was assessed by the BrdUrd Flow Kit (BD Biosciences). Apoptosis was monitored by Annexin V–APC/7-AAD staining (BD Biosciences).

AML cell lines were acquired from DSMZ or ATCC. Cells were maintained in RPMI-1640 medium supplemented with 10%–20% FBS (Life Technologies), used from the 5th to 25th passages, and have been tested for mycoplasma contamination. Immunophenotyping was routinely performed for cellular authentication. Stable luciferase-expressing lines were generated by lentiviral transduction as previously described (44).

### Drug Profiling

Primary myeloblasts ($1 \times 10^5$) or AML cell lines ($5 \times 10^4$) were seeded in the respective culture conditions on 96-well plates (Corning) and treated with DMSO or compounds in the drug panel (from Selleckchem or MedChemExpress) for 72 hours from 0.1 nmol/L to 10 μmol/L. Cell viability was evaluated using CellTiter MTS solution (Promega), with absorbance measured by the Synergy HTX Multi-Mode Reader. Data were normalized against DMSO controls with outliers removed before curve fitting. The AUC and $IC_{50}$ values were calculated from the dose–response curves by nonlinear regression. Whenever the cell viability remained >50% across the entire dose range, the $IC_{50}$ values were designated as the highest dose (i.e., 10 μmol/L) for data formality.

A heat map integrating the AUC values was generated by the pheatmap package in RStudio to visualize the overall drug-sensitivity pattern. Hierarchical clustering was performed using the Euclidean distance metric and Ward's minimum variance method

for linkage (45) to generate drug clusters. To show drugs with similar or dissimilar patterns of sensitivity, Pearson correlation coefficients of AUCs were computed and plotted onto a clustered heat map by RStudio using the corrplot package (46). The presence of synergy in drug combinations was determined using SynergyFinder (47).

### Animal Modeling

Experiments involving animals were conducted in accordance with procedures approved by the Animal Experimentation Ethics Committee. Immunodeficient NOD.Cg-*Prkdc*$^{scid}$/J (NOD/SCID) mice (Jackson Laboratory) were bred by our institutional animal facility. Female, 8- to 11-week-old mice were sublethally irradiated (250 cGy; Gammacell Elite Irradiator, MDS Nordion) and intravenously infused with $5 \times 10^6$ luciferase-expressing AML cells. Transplanted animals were randomized to receive daily intraperitoneal injections of vehicle control (phosphate-buffered saline) or YM155 (2.5 mg/kg, 5 days on 2 days off) for 2 weeks (48), starting on day 3 after transplantation. Venetoclax (100 mg/kg), formulated in 5% DMSO, 30% PEG 400, and 65% Phosal 50 PG, was administered by oral gavage on the same schedule (49). In experiments assessing combinatorial activities of targeted agents with standard chemotherapy, animals were concomitantly administered with intraperitoneal cytarabine (2 mg/kg; ref. 50). The systemic leukemic load was monitored over time using an IVIS 200 System (Xenogen). Prior to imaging, mice were administered with D-Luciferin (150 mg/kg; Promega) and anesthetized with 2.5% isoflurane (Zoetis). Luminescence signals were captured and analyzed as photon emission/second/cm$^2$ using Living Image software (Xenogen). To analyze animal survival, mice reaching humane endpoints (≥20% weight loss, obvious distress, or hindleg paralysis) were sacrificed and regarded as dead.

A more permissive mouse strain, NOD.Cg-*Prkdc*$^{scid}$*Il2rg*$^{tm1Wjl}$/SzJ (NSG), was selected to generate PDXs. Sublethally irradiated female mice of 6 to 8 weeks of age were transplanted with Ficoll-enriched myeloblasts ($2 \times 10^6$–$1 \times 10^7$) via tail veins. At day 3 after transplantation, animals were randomized to receive vehicle solution or single-agent venetoclax as described above. Circulating blasts, defined as human CD45$^+$CD33$^+$CD19$^-$ cells, were monitored serially by flow cytometry. Briefly, 100 μL PB was obtained by tail bleeding followed by red cell lysis. Leukemic cells were detected by flow cytometry using human-specific antibodies. Single-cell suspensions were also prepared from the BM of terminally ill animals to evaluate the impact of drug treatment on medullary leukemia.

### Targeted Sequencing

Genomic DNA was isolated from myeloblasts using the QIAamp DNA Blood Mini Kit (Qiagen). Libraries were prepared with 10 ng DNA using the unique molecular identifier (UMI)-based QIAseq Targeted Human Myeloid Neoplasms Panel (Qiagen). The target captured library was sequenced on the NextSeq 500 system with a Mid Output v2 kit (Illumina). Read processing, alignment (hg19 as the reference), calling, and annotation of single-nucleotide variants/small indels were performed with the UMI-based caller smCounter2 (51) run on GeneGlobe using DNA Variant Calling v2. The filtering strategy for the identification of high-confidence mutations was based on methods described elsewhere (6). Briefly, synonymous variants or variants in introns (except splice donor/acceptor sites) were excluded. Additionally, variants with a VAF <0.05 or a population frequency >0.01 in the 1000 Genomes Project, Genome Aggregation Database, or dbSNP were removed. The remaining variants were visually checked with the Integrative Genomics Viewer. Frameshift, in-frame indels, nonsense mutations, splicing, extension, or missense variants predicted to be detrimental by both SIFT and PolyPhen using the Ensembl Variant Effect Predictor (52) were defined as pathogenic. *FLT3*-ITD was examined by fragment analysis (53), and samples with a mutant/wild-type allelic ratio of ≥5% were considered positive. Recurrent mutations seen in ≥2 patients were kept for analyses. To correlate drug response with gene mutation, one-way ANOVA with type III sums of squares test was performed using drug responses (*Z* scores) as dependent variables and gene mutations as independent variables. The Benjamini–Hochberg method was adopted for multiple comparison correction at a false discovery rate (FDR) of 20% to set the adjusted *P* value cutoff (19).

Sequencing reads of PDX samples were mapped to mouse (mm10) and human (hg19) reference genomes by BWA-MEM (v0.7.15) and GeneGlobe. Mouse-derived reads were removed by Disambiguate (54). Mutations were identified by FreeBayes (v1.3.6) using default parameters, annotated by ANOVAR with databases of 1000 Genomes Project, Exome Aggregation Consortium, COSMIC, and ClinVar (55) and filtered to retain pathogenic, nonsynonymous exonic variants with read depth >250×, MAF <0.01, and VAF >0.05 for downstream analyses. Union of variants in paired samples taken before and after animal grafting were subjected to clonal evolution analysis. SciClone package (v1.1) in RStudio was used to infer subclonal architectures (56). Clonal evolution relationship was mapped by ClonEvol (v0.99.11) (parameters: cluster.center = "mean," num.boots = 1,000, founding.cluster = 1, min.cluster.vaf = 0.05, sum.*P* = 0.01, alpha = 0.05; ref. 57) and visualized by Fishplot package (v0.5.1) in RStudio (58).

### RNA-seq

Total RNA was purified from myeloblasts using TRIzol reagent (Life Technologies) and RNeasy Micro kit (Qiagen). RNA integrity was assessed by the RNA 6000 Pico Kit run on the 2100 Bioanalyzer (Agilent Technologies). Samples with RIN >6 were chemically fragmented, followed by cDNA synthesis and library preparation using the NEB RNA sample preparation kit (Illumina). Sequencing was performed on the NovaSeq 6000 platform (Illumina) to yield 10Gb raw data. Alignment of reads to the reference genome (hg38) was performed using STAR-2.5.3a (59). Reads with <10 counts were excluded, and gene assignments were based on Ensembl genome assemblies. Gene-level counts (CPM) were generated with Partek Flow v10.0 using the RNA-seq pipeline, with DEGs curated by DESeq2 with total coverage ≥10 (60). Gene fusions were retrieved by STAR Fusion (v1.10.0).

### Clinical Implementation

Patients who met the inclusion criteria for personalized treatment—(i) failed two or more previous treatment lines and (ii) no further standard treatments were available—were enrolled to adopt precision medicine on a compassionate basis. Drug profiling results were reviewed by the tumor board comprising expert pediatric oncologists to prioritize the therapeutic options based on (i) drug accessibility, (ii) clinical evidence of safety in children, and (iii) family acceptance of experimental treatment. Morphologic remission was assessed as the standard clinical parameter of disease control. The study is registered at ClinicalTrials.gov (NCT04478006).

### Statistical Analyses

The statistical methods applied for individual experiments are indicated in the figure legends. Analyses were performed with SPSS v25.0, Prism v8.3.1, RStudio v1.3.959, and Origin v9.6.5.169.

### Data Availability

Targeted genome sequencing data were deposited in Sequence Read Archive (SRA; accession number: PRJNA862202). RNA-seq data were deposited in Gene-Expression Omnibus (accession number: GSE192638).

## Authors' Disclosures

C.C. Wang reports grants from the Innovation and Technology Fund and Innovation and Technology Commission during the conduct of the study. R.S. Wong reports grants and personal fees from Novartis, Amgen, GlaxoSmithKline, Janssen, Roche, Sanofi, and Gilead and grants from Pfizer, Astella, Antengene, and Takeda outside the submitted work. J. Huang reports grants from Shenzhen Healthcare Research Project and Sanming Project of Medicine in Shenzhen during the conduct of the study. C.K. Chen reports grants from the National Natural Science Foundation of China, the Shenzhen Healthcare Research Project, the Shenzhen Science and Technology Innovation Commission, and the Sanming Project of Medicine in Shenzhen during the conduct of the study. K.T. Leung reports grants from the Food and Health Bureau, Hong Kong; Children's Cancer Foundation, Hong Kong; Paediatric Bone Marrow Transplant Fund, Hong Kong; Research Grants Council, Hong Kong; Innovation and Technology Commission, Hong Kong; and Sanming Project of Medicine, Shenzhen, China, during the conduct of the study. No disclosures were reported by the other authors.

## Authors' Contributions

**H. Wang:** Conceptualization, data curation, formal analysis, supervision, funding acquisition, validation, investigation, visualization, methodology, writing–original draft, project administration, writing–review and editing. **K.Y.Y. Chan:** Data curation, formal analysis, validation, investigation, visualization, methodology, writing–original draft, writing–review and editing. **C.K. Cheng:** Data curation, formal analysis, validation, visualization, writing–review and editing. **M.H.L. Ng:** Resources, data curation, supervision, investigation, writing–review and editing. **P.Y. Lee:** Data curation, formal analysis, investigation, writing–review and editing. **F.W.T. Cheng:** Resources, supervision, writing–review and editing. **G.K.S. Lam:** Resources. **T.W. Chow:** Resources. **S.Y. Ha:** Resources. **A.K.S. Chiang:** Resources. **W.H. Leung:** Resources, writing–review and editing. **A.Y.H. Leung:** Resources, writing–review and editing. **C.C. Wang:** Resources, writing–review and editing. **T. Zhang:** Resources. **X.-B. Zhang:** Resources, methodology. **C.C. So:** Methodology, writing–review and editing. **Y. Yuen:** Methodology. **Q. Sun:** Formal analysis, investigation, visualization. **C. Zhang:** Investigation. **Y. Xu:** Investigation. **J.T.K. Cheung:** Resources, investigation. **W.H. Ng:** Resources, investigation. **P.M.-K. Tang:** Resources. **W. Kang:** Resources, methodology. **K.-F. To:** Resources. **W.Y.W. Lee:** Resources, methodology, writing–review and editing. **R.S.M. Wong:** Resources. **E.N.Y. Poon:** Resources, writing–review and editing. **Q. Zhao:** Resources. **J. Huang:** Resources, funding acquisition. **C. Chen:** Conceptualization, resources, formal analysis, supervision. **P.M.P. Yuen:** Conceptualization, resources, supervision, funding acquisition, writing–review and editing. **C.-k. Li:** Conceptualization, resources, supervision, funding acquisition, writing–review and editing. **A.W.K. Leung:** Conceptualization, resources, formal analysis, supervision, visualization. **K.T. Leung:** Conceptualization, formal analysis, supervision, funding acquisition, validation, investigation, writing–original draft, project administration, writing–review and editing.

## Acknowledgments

This study was supported by research grants from the Health and Medical Research Fund, Food and Health Bureau, Hong Kong (project no: PR-CUHK-1); the Children's Cancer Foundation, Hong Kong (project no: 6904536); the Paediatric Bone Marrow Transplant Fund, Hong Kong (project no: 7105113); the Theme-based Research Scheme, Research Grants Council, Hong Kong (project no: I12-702/20-N); the Innovation and Technology Fund, Innovation and Technology Commission, Hong Kong (project no: ITS/208/16FX); the Collaborative Research Fund, Research Grants Council, Hong Kong (project no: C5045-20EF); the Health@InnoHK, Innovation and Technology Commission, Hong Kong (Centre for Oncology and Immunology); and the Sanming Project of Medicine, Shenzhen, China (project no: SZSM202011004). The funding bodies were not involved in the study design; the collection, analysis, and interpretation of data; or the decision to submit the manuscript for publication. The authors also thank Ms. Yuk-Lin Yung and Ms. Hoi-Yun Chan for their works on targeted sequencing, and all study participants for their kindness to donate valuable specimens.

The publication costs of this article were defrayed in part by the payment of publication fees. Therefore, and solely to indicate this fact, this article is hereby marked "advertisement" in accordance with 18 USC section 1734.

## Note

Supplementary data for this article are available at Blood Cancer Discovery Online (https://bloodcancerdiscov.aacrjournals.org/).

Received January 19, 2022; revised May 31, 2022; accepted August 9, 2022; published first August 11, 2022.

## REFERENCES

1. Miranda-Filho A, Piñeros M, Ferlay J, Soerjomataram I, Monnereau A, Bray F. Epidemiological patterns of leukaemia in 184 countries: a population-based study. Lancet Haematol 2018;5:e14–24.
2. Rubnitz JE, Kaspers GJ. How I treat pediatric acute myeloid leukemia. Blood 2021;138:1009–18.
3. Zwaan CM, Kolb EA, Reinhardt D, Abrahamsson J, Adachi S, Aplenc R, et al. Collaborative efforts driving progress in pediatric acute myeloid leukemia. J Clin Oncol 2015;33:2949–62.
4. Rasche M, Zimmermann M, Borschel L, Bourquin JP, Dworzak M, Klingebiel T, et al. Successes and challenges in the treatment of pediatric acute myeloid leukemia : a retrospective analysis of the AML-BFM trials from 1987 to 2012. Leukemia 2018;32:2167–77.
5. Kaspers GJ, Zimmermann M, Reinhardt D, Gibson BE, Tamminga RY, Aleinikova O, et al. Improved outcome in pediatric relapsed acute myeloid leukemia: results of a randomized trial on liposomal daunorubicin by the International BFM Study Group. J Clin Oncol 2013;31:599–607.
6. Bolouri H, Farrar JE, Triche T, Ries RE, Lim EL, Alonzo TA, et al. The molecular landscape of pediatric acute myeloid leukemia reveals recurrent structural alterations and age-specific mutational interactions. Nat Med 2018;24:103–12.
7. Chaudhury S, O'Connor C, Cañete A, Bittencourt-Silvestre J, Sarrou E, Prendergast Á, et al. Age-specific biological and molecular profiling distinguishes paediatric from adult acute myeloid leukaemias. Nat Commun 2018;9:5280.
8. Döhner H, Wei AH, Löwenberg B. Towards precision medicine for AML. Nat Rev Clin Oncol 2021;18:577–90.
9. Patel JP, Gönen M, Figueroa ME, Fernandez H, Sun Z, Racevskis J, et al. Prognostic relevance of integrated genetic profiling in acute myeloid leukemia. N Engl J Med 2012;366:1079–89.
10. Papaemmanuil E, Gerstung M, Bullinger L, Gaidzik VI, Paschka P, Roberts ND, et al. Genomic classification and prognosis in acute myeloid leukemia. N Engl J Med 2016;374:2209–21.
11. Burd A, Levine RL, Ruppert AS, Mims AS, Borate U, Stein EM, et al. Precision medicine treatment in acute myeloid leukemia using prospective genomic profiling: feasibility and preliminary efficacy of the Beat AML Master Trial. Nat Med 2020;26:1852–8.
12. Fornerod M, Ma J, Noort S, Liu Y, Walsh MP, Shi L, et al. Integrative genomic analysis of pediatric myeloid-related acute leukemias identifies novel subtypes and prognostic indicators. Blood Cancer Discov 2021;2:586–99.
13. Umeda M, Ma J, Huang BJ, Hagiwara K, Westover T, Abdelhamed S, et al. Integrated genomic analysis identifies UBTF tandem duplications as a recurrent lesion in pediatric acute myeloid leukemia. Blood Cancer Discov 2022;3:194–207.

14. Pikman Y, Tasian SK, Sulis ML, Stevenson K, Blonquist TM, Apsel Winger B, et al. Matched targeted therapy for pediatric patients with relapsed, refractory, or high-risk leukemias: a report from the LEAP Consortium. Cancer Discov 2021;11:1424–39.
15. Letai A. Functional precision cancer medicine—moving beyond pure genomics. Nat Med 2017;23:1028–35.
16. Tyner JW, Tognon CE, Bottomly D, Wilmot B, Kurtz SE, Savage SL, et al. Functional genomic landscape of acute myeloid leukaemia. Nature 2018;562:526–31.
17. Horibata S, Gui G, Lack J, DeStefano CB, Gottesman MM, Hourigan CS. Heterogeneity in refractory acute myeloid leukemia. Proc Natl Acad Sci U S A 2019;116:10494–503.
18. Kurtz SE, Eide CA, Kaempf A, Khanna V, Savage SL, Rofelty A, et al. Molecularly targeted drug combinations demonstrate selective effectiveness for myeloid- and lymphoid-derived hematologic malignancies. Proc Natl Acad Sci U S A 2017;114:E7554–63.
19. Lam SS, Ho ES, He BL, Wong WW, Cher CY, Ng NK, et al. Homoharringtonine (omacetaxine mepesuccinate) as an adjunct for FLT3- ITD acute myeloid leukemia. Sci Transl Med 2016;8:359ra129.
20. Tavor S, Shalit T, Ilani NC, Moskovitz Y, Livnat N, Groner Y, et al. Dasatinib response in acute myeloid leukemia is correlated with FLT3/ITD, PTPN11 mutations and a unique gene expression signature. Haematologica 2020;105:2795–804.
21. Pemovska T, Kontro M, Yadav B, Edgren H, Eldfors S, Szwajda A, et al. Individualized systems medicine strategy to tailor treatments for patients with chemorefractory acute myeloid leukemia. Cancer Discov 2013;3:1416–29.
22. Snijder B, Vladimer GI, Krall N, Miura K, Schmolke AS, Kornauth C, et al. Image-based ex-vivo drug screening for patients with aggressive haematological malignancies: interim results from a single-arm, open-label, pilot study. Lancet Haematol 2017;4:e595–606.
23. Kornauth C, Pemovska T, Vladimer GI, Bayer G, Bergmann M, Eder S, et al. Functional precision medicine provides clinical benefit in advanced aggressive hematological cancers and identifies exceptional responders. Cancer Discov 2022;12:372–87.
24. Malani D, Kumar A, Bruck O, Kontro M, Yadav B, Hellesoy M, et al. Implementing a functional precision medicine tumor board for acute myeloid leukemia. Cancer Discov 2022;12:388–401.
25. Drenberg CD, Shelat A, Dang J, Cotton A, Orwick SJ, Li M, et al. A high-throughput screen indicates gemcitabine and JAK inhibitors may be useful for treating pediatric AML. Nat Commun 2019;10:2189.
26. Cucchi DG, Bachas C, van den Heuvel-Eibrink MM, Arentsen-Peters ST, Kwidama ZJ, Schuurhuis GJ, et al. Harnessing gene expression profiles for the identification of ex vivo drug response genes in pediatric acute myeloid leukemia. Cancers 2020;12:1247.
27. Bruserud O, Gjertsen BT, Foss B, Huang TS. New strategies in the treatment of acute myelogenous leukemia (AML): in vitro culture of AML cells—the present use in experimental studies and the possible importance for future therapeutic approaches. Stem Cells 2001;19:1–11.
28. Larsson P, Engqvist H, Biermann J, Rönnerman EW, Forssell-Aronsson E, Kovács A, et al. Optimization of cell viability assays to improve replicability and reproducibility of cancer drug sensitivity screens. Sci Rep 2020;10:5798.
29. Zhao JC, Agarwal S, Ahmad H, Amin K, Bewersdorf JP, Zeidan AM. A review of FLT3 inhibitors in acute myeloid leukemia. Blood Rev 2022;52:100905.
30. Parry N, Wheadon H, Copland M. The application of BH3 mimetics in myeloid leukemias. Cell Death Dis 2021;12:222.
31. Bill M, Mrózek K, Kohlschmidt J, Eisfeld AK, Walker CJ, Nicolet D, et al. Mutational landscape and clinical outcome of patients with de novo acute myeloid leukemia and rearrangements involving 11q23/KMT2A. Proc Natl Acad Sci U S A 2020;117:26340–46.
32. Liu T, Rao J, Hu W, Cui B, Cai J, Liu Y, et al. Distinct genomic landscape of Chinese pediatric acute myeloid leukemia impacts clinical risk classification. Nat Commun 2022;13:1640.
33. Tang J, Yu J, Cai J, Zhang L, Hu S, Gao J, et al. Prognostic factors for CNS control in children with acute lymphoblastic leukemia treated without cranial irradiation. Blood 2021;138:331–43.
34. Karol SE, Alexander TB, Budhraja A, Pounds SB, Canavera K, Wang L, et al. Venetoclax in combination with cytarabine with or without idarubicin in children with relapsed or refractory acute myeloid leukaemia: a phase 1, dose-escalation study. Lancet Oncol 2020;21:551–60.
35. Chen J, Glasser CL. New and emerging targeted therapies for pediatric acute myeloid leukemia (AML). Children 2020;7:12.
36. Madan V, Koeffler HP. Differentiation therapy of myeloid leukemia: four decades of development. Haematologica 2021;106:26–38.
37. Aung MM, Mills ML, Bittencourt-Silvestre J, Keeshan K. Insights into the molecular profiles of adult and paediatric acute myeloid leukaemia. Mol Oncol 2021;15:2253–72.
38. Chen C, Liu Y, Rappaport AR, Kitzing T, Schultz N, Zhao Z, et al. MLL3 is a haploinsufficient 7q tumor suppressor in acute myeloid leukemia. Cancer Cell 2014;25:652–65.
39. McNeer NA, Philip J, Geiger H, Ries RE, Lavallée VP, Walsh M, et al. Genetic mechanisms of primary chemotherapy resistance in pediatric acute myeloid leukemia. Leukemia 2019;33:1934–43.
40. Diepstraten ST, Anderson MA, Czabotar PE, Lessene G, Strasser A, Kelly GL. The manipulation of apoptosis for cancer therapy using BH3-mimetic drugs. Nat Rev Cancer 2022;22:45–64.
41. Lin A, Giuliano CJ, Palladino A, John KM, Abramowicz C, Yuan ML, et al. Off-target toxicity is a common mechanism of action of cancer drugs undergoing clinical trials. Sci Transl Med 2019;11:eaaw8412.
42. Arber DA, Orazi A, Hasserjian R, Thiele J, Borowitz MJ, Le Beau MM, et al. The 2016 revision to the World Health Organization classification of myeloid neoplasms and acute leukemia. Blood 2016;127:2391–405.
43. Creutzig U, van den Heuvel-Eibrink MM, Gibson B, Dworzak MN, Adachi S, de Bont E, et al. Diagnosis and management of acute myeloid leukemia in children and adolescents: recommendations from an international expert panel. Blood 2012;120:3187–205.
44. Leung KT, Zhang C, Chan KY, Li K, Cheung JT, Ng MH, et al. CD9 blockade suppresses disease progression of high-risk pediatric B-cell precursor acute lymphoblastic leukemia and enhances chemosensitivity. Leukemia 2020;34:709–20.
45. Zhou Q, Yang JJ, Chen ZH, Zhang XC, Yan HH, Xu CR, et al. Serial cfDNA assessment of response and resistance to EGFR-TKI for patients with EGFR-L858R mutant lung cancer from a prospective clinical trial. J Hematol Oncol 2016;9:86.
46. Pesenti C, Navone SE, Guarnaccia L, Terrasi A, Costanza J, Silipigni R, et al. The genetic landscape of human glioblastoma and matched primary cancer stem cells reveals intratumour similarity and intertumour heterogeneity. Stem Cells Int 2019;2019:2617030.
47. Ianevski A, Giri AK, Aittokallio T. SynergyFinder 2.0: visual analytics of multi-drug combination synergies. Nucleic Acids Res 2021;48:W488–93.
48. Minoda M, Kawamoto T, Ueha T, Kamata E, Morishita M, Harada R, et al. Antitumor effect of YM155, a novel small-molecule survivin suppressant, via mitochondrial apoptosis in human MFH/UPS. Int J Oncol 2015;47:891–9.
49. Bisaillon R, Moison C, Thiollier C, Krosl J, Bordeleau ME, Lehnertz B, et al. Genetic characterization of ABT-199 sensitivity in human AML. Leukemia 2020;34:63–74.
50. Yang C, Boyson CA, Di Liberto M, Huang X, Hannah J, Dorn DC, et al. CDK4/6 inhibitor PD 0332991 sensitizes acute myeloid leukemia to cytarabine-mediated cytotoxicity. Cancer Res 2015;75:1838–45.
51. Xu C, Gu X, Padmanabhan R, Wu Z, Peng Q, DiCarlo J, et al. Smcounter2: an accurate low-frequency variant caller for targeted sequencing data with unique molecular identifiers. Bioinformatics 2019;35:1299–309.
52. McLaren W, Gil L, Hunt SE, Riat HS, Ritchie GR, Thormann A, et al. The ensembl variant effect predictor. Genome Biol 2016;17:122.
53. Stone RM, Mandrekar SJ, Sanford BL, Laumann K, Geyer S, Bloomfield CD, et al. Midostaurin plus chemotherapy for acute myeloid leukemia with a FLT3 mutation. N Engl J Med 2017;377:454–64.

54. Ahdesmäki MJ, Gray SR, Johnson JH, Lai Z. Disambiguate: an open-source application for disambiguating two species in next-generation sequencing data from grafted samples. F1000Res 2016; 5:2741.
55. Wang K, Li M, Hakonarson H. ANNOVAR: functional annotation of genetic variants from high-throughput sequencing data. Nucleic Acids Res 2010;38:e164.
56. Miller CA, White BS, Dees ND, Griffith M, Welch JS, Griffith OL, et al. SciClone: inferring clonal architecture and tracking the spatial and temporal patterns of tumor evolution. PLoS Comput Biol 2014;10:e1003665.
57. Dang HX, White BS, Foltz SM, Miller CA, Luo J, Fields RC, et al. ClonEvol: clonal ordering and visualization in cancer sequencing. Ann Oncol 2017;28:3076–82.
58. Miller CA, McMichael J, Dang HX, Maher CA, Ding L, Ley TJ, et al. Visualizing tumor evolution with the fishplot package for R. BMC Genomics 2016;17:880.
59. Dobin A, Davis CA, Schlesinger F, Drenkow J, Zaleski C, Jha S, et al. STAR: ultrafast universal RNA-seq aligner. Bioinformatics 2013;29: 15–21.
60. Anders S, Huber W. Differential expression analysis for sequence count data. Genome Biol 2010;11:R106.